Engineering collagen-based vascular substitutes that recapitulate native vessel structural and functional properties

By

Constantine Tarabanis

Beth Israel Deaconess Medical Center
Department of Surgery
Adviser: Elliot L. Chaikof MD, PhD

Submitted in Partial Fulfillment of the Requirements for the M.D. Degree
with Honors in a Special Field at Harvard Medical School

02/10/2020

Table of Contents

Abstract

Autologous vein grafts remain the gold standard in small diameter bypass grafting for the surgical management of peripheral arterial and coronary artery disease. Yet outcomes remain compromised by low patency rates. Tissue-engineering strategies have been explored as alternatives, however, a clinically available tissue engineered vascular graft (TEVG) remains an elusive reality. In the present study we report a novel fabrication method for the generation of TEVGs. A microfluidic strategy is employed for the rapid and continuous formation of ultrathin, highly aligned and compacted collagen sheets with tunable properties. In turn, these collagen sheets were used to fabricate TEVGs yielding tubular structures comprised of circumferential human aortic smooth muscle cell layers alternating with layers of compact, aligned and genipin-crosslinked collagen fibrils. The resulting TEVGs recapitulated aspects of both the microstructure and mechanical properties of native arteries. The maximum burst pressure and suture retention strength averages achieved were 2,645 ± 346 mm Hg and 153.5 ± 37.4 gF, respectively. Importantly, the present TEVG approach does not make use of synthetic polymers or prolonged bioreactor incubation times, hence being a more cost-effective and scalable solution.

Acknowledgements

I wish to thank my mentor and Principal Investigator of this study, Dr. Elliot Chaikof, for giving me the opportunity to contribute to this project and for his unceasing support and guidance. His willingness to listen, his ability to explain scientific concepts and his kind personality will not be forgotten. I would also like to thank David Miranda Nieves for the experimental training he offered, as well as his continued guidance throughout my time in the lab. I am also grateful to Dr. Carolyn Haller, Dr. Daniel Wong, Dr. Erbin Dai, Dr. Liying Liu and the Günther group of the University of Toronto for their contributions to this project. Lastly, I would like to thank all members of the Chaikof lab for their support: Dr. Walter Wever, Dr. Simon Park, Dr. Oki Ham, Dr. Jiaxuan Chen, Dr. Diane Park and Dr. Appi Mandhapati.

Glossary of abbreviations

CABG = coronary artery bypass grafting

C-terminus = carboxyl-terminus

E = elastic (or Young's) modulus

ECM = extracellular matrix

FFB = flow focusing buffer

FPB = fibrillogenesis promoting buffer

FWHM = full-width-half-maximum

g = gram

gF = gram-Force

Gly = glycine

HAoSMC = human aortic smooth muscle cell

H&E = hematoxylin and eosin

ID = inner diameter

kDa = kiloDalton

μm = micrometer

mg = milligram

mL = milliliter

mm = millimeter

mm Hg = millimeters of mercury

MW = molecular weight

NA = numerical aperture

nm = nanometer

N-terminus = amino-terminus

OD = outer diameter

PAD = peripheral arterial disease

PBS = phosphate-buffered saline

PEG = polyethylene glycol

PTFE = polytetrafluoroethylene

SMC = smooth muscle cell

SRS = suture retention strength

TEM = transmission electron microscopy

TEVG = tissue-engineered vascular graft

UTS = ultimate tensile strength

Introduction

Collagen biosynthesis

Cells and extracellular matrix (ECM) are the two main components of tissues in the body. The ECM is an interconnected series of macromolecules, which includes proteins and carbohydrates. Collagen and elastin are the first and second most abundant ECM macromolecules respectively, with the former constituting up to 30% of the total dry mass in mammals[1,2]. From a functional perspective, elastin provides tissue elasticity and resilience, whereas collagen contributes to structural support and local biological interactions[3].

Among the twenty-eight genetically distinct collagen types identified to date, focus will be placed on the most common type, fibril-forming collagens (types I, II, III, V, and XI)[4,5]. Despite contributions by other cell types, fibroblasts account for the majority of collagen production[6]. Collagen propeptide synthesis through mRNA translation occurs in the rough endoplasmic reticulum and the resulting molecules are post-translationally modified through glycosylation and hydroxylation[7]. Hydroxylase enzymes along with cofactors (ferrous ions, oxygen, and ascorbate) hydroxylate proline and lysine, which occupy positions X and Y in collagen's repeating sequence $(Gly\text{-}X\text{-}Y)_n$[7]. These post-translational modifications are critical for intramolecular hydrogen and disulfide bond creation and the consequent self-assembly into triple helices of three collagen α-chains (procollagen) that occurs in the Golgi apparatus[8]. Procollagen is secreted from the Golgi apparatus and extracellularly cleaved at the C- and N-terminals yielding the insoluble tropocollagen[9].

Following exocytosis into the extracellular space and proteolytic processing, many staggered tropocollagens self-assemble into fibrils through the entropy-driven process of fibrillogenesis [9]. In turn, these collagen fibrils combine through non-covalent bonds and covalent lysine-hydroxylysine cross-linkages catalyzed by copper-containing lysyl oxidase[9]. The resulting collagen fibrils have diameters ranging from 10 to 300 nm and a banding pattern with a characteristic length scale of 54–67 nm, known as D-periodicity[10,11,12]. In the wide array of tissues containing collagen as a basic structural element (cornea, tendon, vascular wall), higher order collagen fibril organization into fibers is tissue-dependent and closely linked to tissue function[2].

Fabrication of collagen biomaterials

Naturally derived biomaterials, like collagen and elastin, pose a unique opportunity having exhibited limited evidence of immunogenic reactions and local/systemic toxicity, as well as not requiring extensive modification to promote cell adhesion, proliferation, and migration[13,14]. This fact in combination with collagen's extensive structural and functional significance in living tissues, has rendered collagen a widely used biomaterial in the fields of drug delivery and tissue engineering. Indeed, collagen and in some cases elastin as well, have been used for the tissue engineering of vascular grafts, cardiac tissue, cartilage, tendons, ligaments, skin and liver constructs[15].

The source of collagen molecules has been primarily two-fold: animal-derived and recombinant. Porcine skin, bovine tendon, rat tail and other animal sources have been used for the extraction of collagen, particularly type I[16]. The aforementioned process of

collagen biosynthesis in mammals results in collagen fibril formation, however mature fibrils have chemical cross-links that limit their aqueous solubility. Hence, tissues of younger mammals are the preferred collagen source[17,18]. Limitations of animal-derived collagen include ethical concerns with the harvesting process, batch-to-batch variability and the requirement for good manufacturing practices to address contamination risks[16]. In response, recombinant human collagen has been expressed in yeast, *Escherichia coli*, mammalian cells and other platforms[19]. However, applications of recombinant human collagen have remained limited due to two main drawbacks. Firstly, recapitulation of post-translational modifications has been a challenge[19], although the addition of prolyl-4-hydroxylase coding domains to recombinant sequences has addressed at least proline hydroxylation[20,21,22]. Secondly, the high production cost of this research method has outweighed benefits, such as control over amino acid sequence and chain length[23].

Fabrication methods of collagen biomaterials have included casting, bioprinting and fiber spinning. In biomaterial manufacturing, casting involves pouring viscous polymer solutions into molds[24] and in the case of collagen has been used to fabricate planar and tubular scaffolds[25,26,27]. Collagen scaffolds have also been generated through inkjet (via both pH-[28,29] and temperature-triggered[30] gelation) and laser-assisted[31,32] bioprinting. Yet, most bioprinting efforts have also included non-naturally derived molecules to facilitate cell growth and mechanical integrity[15]. Consequently, deposited cells need to reconstitute tissue through synthesis of structural proteins (like collagen and elastin) either following implantation or while the construct is maintained in a bioreactor[15]. This process takes months and has limited these fabrication methods[15]. A significant limitation of both casting

and bioprinting has also been the inability to control fibrillar alignment and compaction. This has resulted in collagen constructs with mechanical properties insufficient to withstand physiologically relevant loading forces[27,15].

Comparatively, fiber spinning has afforded researchers some control over fibrillar alignment and compaction. Among fiber spinning approaches, both wet spinning[33,34] and electrospinning[35,36,37,38,39,40,41] have been used to generate collagen (as well as elastin) fibers either in isolation or in combination with other biomaterials. In addition to this method, induction of some level of collagen fibrillar alignment and compaction has also been achieved via strain[42], spatial confinement[43,44], fluid flow-induced shear stress[43,45,46,47], electric[48,49] or magnetic fields[50,51,52] and microfluidic channel systems[47,53,54]. Still the aforementioned methods, including fiber spinning, have their limitations. There is still limited control over collagen fibrillar alignment or compaction, and this control is delivered only in one-dimensional or substrate-attached two-dimensional structures. Also, many of these methods are not scalable to the extent necessary for the purposes of tissue engineering. In the present study we report the adaptation of a microfluidic system for the continuous formation of three-dimensional collagen structures with precise control over both collagen alignment and compaction. Collaborators on the present project, Dr. Günther's group of the University of Toronto, first developed this system for the continuous formation of planar biomaterial hydrogels (including collagen) without the need for substrate support[55].

Properties of native blood vessels

The vascular wall is comprised of three concentric layers or tunicae. A non-thrombogenic monolayer of endothelial cells forms the innermost layer, the tunica intima[56]. The tunica adventitia, the outermost layer, is composed of fibroblasts and a collagenous extracellular matrix[56]. Between these two layers lies the tunica media, which is separated from the tunica intima by an internal elastic lamina and whose primary cellular composition is concentrically organized smooth muscle cells (SMCs)[56]. Vascular SMCs exist in a phenotypic continuum, which shifts according to prevailing conditions[57]. Under physiologic conditions, they possess a quiescent contractile phenotype, regulating blood flow through dilation and constriction of blood vessels[56,57]. Under pathological conditions, such as vascular injury, vascular SMCs convert to a synthetic and non-contractile phenotype characterized by proliferation and increased matrix production[56,57].

Both collagen and elastin are key functional and structural components of the vascular wall. Elastin is concentrated in the tunica media, either as elastin fibers in muscular arteries[58] or elastin fibers arranged in concentric rings of elastic lamellae in elastic arteries[56]. Elastic lamellae allow elastic arteries, such as the aorta and its largest branches (brachiocephalic, common carotid, subclavian and iliac arteries), to maintain sufficient blood pressure throughout both cardiac systole and diastole[59]. More broadly, elastin contributes to blood vessels' elastic properties and along with collagen, prevents pulsatile blood flow from irreversibly deforming the vascular wall[56,60]. Collagen, particularly types I and III[56], is distributed throughout the three layers and functions to prevent vascular wall rupture by providing tensile stiffness[56,60]. The tissue-specific higher

order organization of collagen fibrils in the vascular wall involves 30 – 100 nm[61] collagen fibrils arranged in 1.8 to 10 µm diameter fibers[62,63]. These collagen fibers are in turn circumferentially aligned at angles of 18.8° – 58.9° for human aorta[2] and 2° – 83° for saphenous vein[64]. This structural arrangement of collagen fibrils contributes to the mechanical properties required by blood vessels to tolerate physiologic blood pressures[65,66].

Among these mechanical properties, burst pressure, suture retention strength (SRS) and compliance are often used to characterize both native and tissue engineered blood vessels[67]. Burst pressure has typically been defined as the pressure at which a blood vessel ruptures after continuous inflation at a steady rate[67]. Suture retention strength is calculated by measuring the force required to remove a suture placed at the end of a vessel sample and is expressed in units of gram-Force (gF)[67]. Compliance is calculated from the percent change in internal radius over a range of pressures and expressed in units of %/100 mm Hg[67]. In humans, burst pressure values for popliteal arteries range from 2,200 to 4,225 mm Hg[68,69] and for saphenous veins from 1,600 to 2,500 mm Hg[68,69,70,71]. Suture retention strength has been reported for internal thoracic arteries at 88 – 200 gF[70,72] and for umbilical veins at 180 – 250 gF[69,70,71]. Coronary arteries possess a high arterial compliance at 8.0 – 17.0 %/100 mm Hg[73,74] compared to popliteal (4.7 – 8.5 %/100 mm Hg[75]) and internal thoracic arteries (6.5 – 12.0 %/100 mm Hg[68,72]).

Tissue engineered vascular grafts

A wide array of research efforts have been made to tissue engineer vascular grafts that to some extent recapitulate the aforementioned native structural and functional properties of blood vessels[67,76,77]. The traditional "cells-plus-scaffold" tissue engineering concept was first applied to blood vessels by Weinberg and Bell in 1986[27]. A casted collagen hydrogel cultured with SMCs and endothelial cells afforded burst pressures between 100 and 200 mm Hg, necessitating the addition of a Dacron mesh to reach maximum pressures in the range of 300 to 400 mm Hg[27]. Since then, efforts for the generation of TEVGs have included both scaffold and scaffold-free tissue engineering approaches.

Sheet-based tissue engineering, first pioneered by L'Heureux and Auger in 1998[78], has been the main scaffold-free approach to TEVGs. The main principle underlying this approach is that SMCs and fibroblasts form cohesive and detachable cell sheets with prolonged culturing (approximately 30 days) in ascorbic acid-containing media[78]. These sheets were wrapped about a tubular support to form circumferential layers composed entirely of secreted matrix proteins and either SMCs or fibroblasts, resembling the native tunica media and adventitia respectively[78]. The resulting TEVGs exhibited promising *in vitro* mechanical properties including burst pressure of 3,000 – 4,000 mm Hg and SRS of 140 – 180 gF, but a compliance of approximately 1.5% for a pressure change from 80 to 120 mm Hg[70]. Importanly, these TEVGs exhibited some promising clinical results when implanted as arteriovenous fistulas in high-risk patients[79,80]. The use of human mesenchymal stem cells in sheet-based tissue engineering[81] has shown the versatility of this approach, however challenges remain. The long culture times (about 28 weeks[78]) have

kept costs high and limited any potential clinical applications to non-urgent indications[67]. The aforementioned TEVG implantation in humans as arteriovenous fistulas has shown evidence of graft failure and a need for re-intervention even among a small, yet high-risk, cohort of ten patients[79]. Although sheet-based tissue engineering remains a key scaffold-free approach, novel scaffold-free methods have also emerged, for example with the use of periodic high hydrostatic pressure[82] and bioprinting[83].

Scaffold tissue engineering approaches have utilized synthetic, biomaterial-based or decellularized tissue scaffolds (or a combination of the above). As the name suggests, decellularized tissue scaffolds involve decellularizing a tissue, while maintaining its native extracellular matrix that provides a structural base for seeding with cell types of preference[67]. Although some have originated from humans (such as umbilical arteries[84]), the vast majority of decellularized tissues have come from animals, such as canine carotid arteries[85,86], jugular veins[71] and ureters[87], rat abdominal aortas[88], porcine aortas[89,90,91], carotid arteries[92,93], small intestine segments[94] and ureters[95], as well as bovine ureters[96]. Resulting TEVGs have demonstrated promising *in vitro* mechanical properties, as for example decellularized porcine carotid artery-derived grafts possessing burst pressures of 1,000 – 2,000 mm Hg, SRS of 300 gF, but a compliance of 5.8% for a pressure change from 0 to 200 mm Hg[93]. Yet clinical data from the case of decellularized bovine ureters have been concerning due to aneurysmal formation[97], poor long-term patency (14% at one year) as hemodialysis shunts[98], as well as inflammation and infection likely due to residual xenoantigen[99].

Biodegradable synthetic polymer scaffolds have been extensively studied, including polycaprolactone[100,101], polyglycolic acid[102,103,104,105,106], polylactic acid[107], polyurethane[108], and related copolymers or composites[109]. These synthetic scaffolds are bioresorbable and are typically pre-seeded with cells, conditioned in a bioreactor and implanted in animal models[67]. Post-implantation, some *in situ* regeneration of the vascular wall by migration of adjacent cells or homing of circulating progenitors can be expected[67]. Since their first publication in 1999[102], the Niklason group has been a pioneer of this tissue engineering approach having generated, among others, a polyglycolic acid scaffold-based TEVG with burst pressures of 1,000 – 2,000 mm Hg and SRS of 40 – 50 gF[106]. Using this tissue engineering approach, some measure of clinical success has been observed[107,110] as for example in pediatric populations where TEVGs were implanted as extracardiac cavopulmonary conduits[111]. However, in a clinical study by the Niklason group in a larger cohort of adult patients, synthetic scaffold-based TEVGs exhibited primary patency at 12 months of 28%, due to graft thrombosis[112].

Collagen alone[27] or in combination with elastin[113,114,115,116] has been widely used for the generation of biomaterial-based TEVG scaffolds. Other efforts have involved the use of fibrin or combinations of these biomaterials with synthetic polymers[117]. The fabrication methods of collagen biomaterials and their limitations have been covered above, but among them electrospinning[34],[115] and casting[27,67] have been primarily employed in the field of TEVG. Our laboratory, the Chaikof group, has made particular progress with this tissue engineering approach. More specifically, a biomaterial composite of crosslinked, oriented collagen microfibers reinforcing a recombinant elastin matrix yielded TEVGs with an

approximate burst pressure of 1,500 mm Hg, SRS of 170 gF and compliance of 5.1%/100 mm Hg[34].

Challenges to the clinical implementation of all aforementioned tissue engineering approaches have remained, including the possibility of scalable production, requirements for prolonged incubation times[78], graft aneurysmal dilation and thrombosis [79,97], post-implantation neointimal hyperplasia[84] and poor long-term patency rates[98,112]. A mismatch of biomechanical properties between endogenous vessels and grafts could explain some of these phenomena, such as a compliance mismatch leading to neointimal hyperplasia[67]. Hence, despite this impressive progress made over the past 30 years, a clinically available TEVG remains an elusive reality. We hypothesize that this is due to the sustained inability to truly recapitulate the native microstructure of the blood vessel wall components, such as collagen fibrillar alignment and compaction. Hence, here we report the use of the aforementioned microfluidic system[55]-derived collagen sheets for the generation of TEVGs.

Clinical significance

Over 71 million people in the United States alone are affected by cardiovascular disease, accounting for over 7 million annual inpatient visits, over 450,000 bypass surgeries and costs exceeding 500 billion dollars annually[118]. Cardiovascular disease also encompasses peripheral arterial disease (PAD), a state of reduced blood flow to lower extremities due to the progressive narrowing of arteries most commonly caused by atherosclerosis[119]. PAD-related morbidity can range from no symptoms, to lower extremity pain, to limb ischemia necessitating amputation[120]. Although prevalence estimates have

fluctuated depending on the diagnostic method employed, PAD affects up to 14% of the general population and up to 20% of individuals over the age of 75[121,122]. PAD though does not usually appear in isolation, having been consistently associated with coronary heart disease and stroke, as well as increased all-cause and cardiovascular mortality[120,123]. Medical therapy, vascular bypass grafting and angioplasty with or without stenting are included in the therapeutic armamentarium for cardiovascular disease, including PAD[67].

Synthetic polymer prosthetics, like Dacron and polytetrafluoroethylene, have exhibited long-term patency in their now established use for the replacement of large diameter vessels (>6 mm), such as the aorta[67]. However, within the cardiac, peripheral and cerebral vasculature most blood vessels have diameters of less than 6 mm[67]. As described above, small diameter synthetic polymer-based vascular grafts have exhibited poor patency rates[98,112], neointimal hyperplasia and thrombosis[84]. Hence, autologous vein grafts remain the gold standard in small diameter bypass grafting, comparatively exhibiting the best patency rates for cardiac and peripheral bypass grafting[124].

However, autologous vein grafts also have important limitations. Firstly, bypass grafting is more prevalent in patients over the age of 65 years, who are also less likely to have sufficient vein for autologous grafting[67]. Such autograft suitability is also currently difficult to define with certainty in advance of bypass operations[67]. Secondly, despite their comparative superiority, autologous veins' patency rates are still affected by stenosis and occlusion. For example, a multicenter, prospective study of 1,404 patients with severe PAD demonstrated primary patency of 60% at 1 year for vein grafts used in infrainguinal revascularization[124]. Vein graft stenosis or occlusion in lower extremities can rise up to

50% within 3 to 5 years[124,125,126]. In the related field of coronary artery bypass grafting (CABG), a prospective study of 3,014 patients undergoing first-time CABG with saphenous vein, experienced >75% stenosis or occlusion, in 40-50% of autologous vein grafts[127]. The subsequent potential need for reintervention compounds the operative morbidity in an already high-risk[120,123] surgical population.

Consequently, there is a clinical need for small diameter (<6 mm) vascular grafts to improve upon the failure of synthetic polymer TEVGs and the circumscribed success of autologous vein grafts. This has been a pivotal clinical driving force for the field of TEVGs, as well as for the present study.

Materials and Methods

Isolation and purification of collagen

Acid-soluble, monomeric rat-tail tendon collagen (MRTC) was obtained from Sprague-Dawley rat tails following Silver and Trelstad[128]. After thawing frozen rat tails (Pel-Freez Biologicals, Rogers, AK) at room temperature, tendons were extracted using a wire stripper, placed in HCl (10 mM, pH2; 150 mL per rat tail) and stirred for 4 h at room temperature. The dissolved collagen was separated by centrifugation at 30,000 g and 4°C for 30 minutes followed by sequential filtration through 20 µm, 0.45 µm, and 0.2 µm membranes. Collagen was in turn precipitated with the addition of NaCl in HCl (pH2) to an 0.7 M net salt concentration, followed by 1 h stirring and 1 h centrifugation at 30,000 g and 4°C. The precipitated collagen was re-dissolved in HCl (10 mM) overnight and the resulting solution dialyzed against phosphate buffer (20 mM) for at least 4 h at room temperature. Additional dialysis was performed against phosphate buffer (20 mM) at 4°C for at least 8 h, and against HCl (10 mM) at 4°C overnight. The final MRTC solution was frozen and lyophilized. The lyophilized type I monomeric collagen was dissolved in deionized water (pH 2) at a 5 mg/mL concentration. Blue food dye (Club House, Canada) was added for the purposes of visualization. The solution was stirred continuously at 4°C for 24 h yielding an acidic collagen solution.

Preparation of buffer solutions

The Flow Focusing Buffer (FFB) comprised a neutralization buffer prepared in deionized water to induce rapid gelation of the collagen solution. It contained

polyethylene glycol (PEG, 10 wt%, MW 35 kDa, Sigma Aldrich), TES (6.86 mg/mL, Sigma Aldrich), monobasic sodium phosphate (4.14 mg/mL, Sigma Aldrich), dibasic sodium phosphate (12.1 mg/mL, Sigma Aldrich), and sodium chloride (7.89 mg/mL, Sigma Aldrich). The pH of the solution was adjusted to 8[129]. The Fibrillogenesis Promoting Buffer (FPB) comprised a phosphate buffer prepared in deionized water to induce fibrillogenesis. It contained Tris (10 mM, Sigma Aldrich), dibasic sodium phosphate (4.26 mg/mL, Sigma Aldrich) and sodium chloride (7.89 mg/mL, Sigma Aldrich)[130].

Aligned collagen sheet formation and crosslinking

The microfluidic devices were fabricated using multilayer soft lithography as previously described[55] and were supplied by the collaborating Günther group of the University of Toronto. The extrusion reservoir was filled with FFB until the center of the mandrel cross-sectional area was reached (*Figures 1* and *2*). Then rat tail type I collagen dissolved in deionized water (pH 2) at a 5 mg/mL concentration, and FFB were co-extruded through the three-layered microfluidic device (*Figure 1b, c*) at a flow rate of 400 µL/min and 4,000 µL/min, respectively. Injection of these solutions into the microfluidic device was achieved using disposable plastic syringes, Tygon PVC clear tubing (ID 1/16", OD 1/8", McMaster Carr, CA, USA), and two infusion pumps (model PHD 2000, Harvard Apparatus, Holliston, MA, USA). With the top half of the constriction bracket (noted as 1 in *Figure 2*) removed, the collagen sheet emerging at the device outlet was manually guided using tweezers past the bottom half of the constriction bracket and placed over the computer-controlled mandrel (*Figures 1* and *2*). Following manual placement of the top

half of the constriction bracket and initiation of mandrel rotation, tweezers were again used to prevent the extruding sheet from wrapping around the mandrel. Upon achieving the desired sheet length, the rotating mandrel was stopped, and the resulting, continuous collagen sheet incubated in the FFB-filled reservoir for 30 minutes. To obtain a 70 cm long sheet approximately 1 mL of acidic solution was required.

The resulting continuous collagen sheet was manually cut with scissors into 23 cm long segments. Each 23 cm long segment was manually spread over custom-made 23 cm long glass slides using tweezers, washed 3x with deionized water and air-dried for at least 15-30 min. Two and three collagen sheets were spread sequentially on top of each other (stacking) to yield bilamellar and trilamellar structures, respectively. In turn, the collagen sheets (single, bilamellar or trilamellar) were transferred to FPB for a 48 h incubation at 37°C. Where specified, single and multilamellar sheets were crosslinked to improve sheet biostability. Briefly, sheets were incubated at 37°C for 1 h in genipin (Wako Chemicals, Richmond, VA) at a concentration of 6 mg/mL and then washed with deionized water 3x. Genipin was first dissolved in 50% ethanol buffer 10-times concentrated (or 60 mg/mL) and then diluted to a final concentration of 6 mg/mL with the addition of phosphate-buffered saline (PBS, Sigma Aldrich). For the purposes of the acid solubility test (*Figure 5a*), collagen sheets serving as a positive control were instead crosslinked with glutaraldehyde (1% v/v in PBS) at 37°C for 24 h. For the purposes of the acid solubility test (*Figure 5a*) Genipin or glutaraldehyde crosslinked, or untreated collagen sheet samples were dried on glass slides, and then weighed, W_i. Samples were then incubated

for 24 h in an acidic solution (pH 2) at 37°C, and then weighed post-incubation, W_f. Percentage extractables were calculated by: Extractable (%) $= \frac{(W_i - W_f)}{(W_i)} \times 100$.

Sheet thickness and width measurement

For the purposes of sheet thickness measurements, collagen sheets were incubated for 1 h at room temperature in Picro-Sirius Red Solution (ab246832, Abcam, Cambridge, MA), using enough volume to completely cover each collagen sheet. The collagen sheet samples were then washed with acetic acid 2x and with PBS 1x in that order. Samples were then spread on coverslips (No 1, thickness = 0.13 mm, width and length = 22 mm, Fisherfinest Premium superslip), rehydrated prior to imaging and imaged using a Zeiss 710 confocal laser scanning microscope with a 40x or 63x oil immersion objective (NA = 1.30, depth field = 0.25 µm, and field of view = 250 µm x 250 µm) in the FITC channel (excitation: 490 nm, emission: 520 nm). Z-stack image slices with a step size of 0.1 µm were obtained. Image analysis was performed with a custom ImageJ macro, which set a threshold for "meaningful" signal at 50% the maximum intensity at every z-point across the stack. Thickness at every z-point across the stack was calculated by the macro by subtracting the threshold value from the maximum intensity. The ImageJ macro then calculated sheet thickness by averaging the thickness at every z-point across the stack (*Figures 3b* and *5e*). For the purposes of sheet width measurements, collagen sheets were incubated for 1 h at room temperature in fluorescein isothiocyanate-dextran solution and washed with deionized water 3x. Sheet width was determined by obtaining *x-y* tiles with 10% overlap, using ImageJ to measure the sheet width (*Figure 3c*).

Transmission electron microscopy

Dry collagen sheet samples were washed 3x in cacodylate buffer (0.1 M) at pH 7.4, and fixed in glutaraldehyde (2.5%) and paraformaldehyde (2%) in cacodylate buffer (0.1 M) at pH 7.4 for 90 min. Samples were washed 3x in cacodylate buffer (0.1 M) at pH 7.4 once again, as well as 3x with deionized water. Samples were fixed with osmium tetraoxide (1%) in cacodylate buffer (0.1 M) at pH 7.4 for 1 h. *En bloc* staining was accomplished using uranyl acetate (2%) in deionized water for 1 h. In turn, samples were washed in deionized water, dehydrated with the use of a series of ethanol solution concentrations (25-100%), and then embedded in Quetol/Spurr resin at 30% overnight, 67% for 8 h, 100% overnight, and polymerized in an oven at 60°C for 48 h. Post-staining was accomplished with uranyl acetate (5%) for 15 min , followed by Reynolds lead citrate for 15 min. Throughout this process and to ensure a well-defined sheet orientation (no folds or wrinkles, flat), the sheet was placed between two rectangular, centrally slotted PEEK pieces. A scalpel was used to cut out the resin-embedded sheet within the central slot, which was cut with a microtome (model Leica Ultracut RMC MT-6000 ultramicrotome) into 60 – 80 nm thin sections and imaged with a transmission electron microscope (model FEI Tecnai 20, Nanoscale Biomedical Imaging Facility, SickKids Hospital, Toronto, Canada, 120 kV).

Image analysis yielded measurements for fibril diameter, fibril density and angular alignment. Fibril diameters at different V^* values were obtained using Nikon's NIS Elements Advanced Research (AR) Software (Version 4.13, Nikon instruments Inc., Melville, NY, USA). Each data point represents an average value of five images and at least

15 fibrils per image. Collagen fibril density was calculated by dividing the sum of collagen fibril area in a TEM image by the total image area. Angular alignment was obtained by first converting the TEM images to binary images, applying a Fast Fourier Transform algorithm to an oval profile and conducting a 'radial sum' analysis over 180 points in ImageJ. The data was shifted 90° to obtain a central frequency peak for plotting the percentage of aligned fibrils as frequency (%) as a function of the angle of alignment. Full Width at Half Maximum (FWHM) was calculated from the difference between angles of alignment at which the frequency of alignment was half.

Collagen sheet mechanical testing

The tensile properties of rehydrated collagen sheets were measured using a Dynamic Mechanical Thermal Analyzer V (DMTA V, Rheometric Scientific, Piscataway, NJ), with a 15 N load cell in the inverted orientation to facilitate hydrated measurements as previously described[33]. Briefly, collagen sheets (10 mm x 20 mm) were immersed in a PBS bath at 37°C for 15 min and preconditioned by 15 cycles up to 66% of the average maximum failure strain. Testing involved straining at 4 mm/min until fracture of the collagen sheet and mechanical properties (ultimate tensile strength, elastic modulus, and strain to failure) were calculated from the stress-strain curve, using the already determined sheet dimensions (length, width, thickness).

Cell culture

Human aortic smooth muscle cells (HAoSMCs) were purchased from Lonza (Walkersville, MD), and cultured at 37°C and 5% CO_2. They were cultured in medium consisting of high-glucose Dulbecco's modified Eagle's medium (DMEM) with serum (20%), insulin (0.13 U/mL), epidermal growth factor (EGF, 0.5 ng/mL), basic fibroblast growth factor (bFGF, 10 ng/mL), penicillin G (10,000 U/mL), copper sulfate (3 ng/mL), L-proline (50 ng/mL), L-alanine (40 ng/mL), and glycine (50 ng/mL). HAoSMCs prior to passage 9 were utilized for all experiments.

TEVG fabrication and histology

The process of fabricating the TEVGs is summarized in *Figure 6a*. Briefly, aligned collagen sheets (L = 23 cm, W = 1.5 cm) were extruded, spread over glass slides, stacked in the case of bilamellar and trilamellar constructs, incubated in FPB for 48 h and genipin (6 mg/mL) crosslinked as described above under "*Aligned collagen sheet formation and crosslinking*". Importantly, only collagen sheets extruded at V^* = 10 were used for TEVG fabrication. HAoSMCs were cultured as above, seeded at a density of 40,000 cells/cm^2 and allowed to incubate in their culture medium for 72 hours. The resulting cell-seeded collagen sheets were rolled around removable mandrels (Φ = 1.5 mm) using a custom-built setup comprised of a conveyor belt and rolling domain (*Figure 6b*). Conveyor belt and mandrel velocities were fixed constant at 0.25 mm/s and 0.24 mm/s, respectively. The velocity differential was established to ensure tension in the sheet for successful rolling, while avoiding sheet rupture. After rolling, the resulting tubular constructs were

incubated (with the rolling mandrel) for an additional 7 days in full media supplemented with 50 µg/mL ascorbic acid, which was replaced 3x during that week. Following mandrel removal, the TEVG were ready for mechanical testing.

For the purposes of histological analysis, freshly-fabricated TEVGs and freshly-harvested Wistar rat abdominal aorta samples were fixed using 10% buffered formalin, paraffin-embedded and section at 5 µm thickness. Histological evaluations of the cross-sections were achieved with hematoxylin and eosin (H&E) staining (Abcam, Cambridge, MA).

TEVG mechanical testing

Burst pressure, suture retention strength and compliance measurements were made using experimental setups akin to ones previously described by our group[34,131]. Burst pressure and compliance measurements were obtained with the use of a custom-made setup and at a constant inflation rate of 2 mL/min and temperature of 37°C. The TEVGs were cannulated to this experimental setup consisting of a syringe pump (model PHD 2000, Harvard Apparatus, Holliston, MA, USA), a pressure transducer (WIKA, Lawrenceville, GA) and a 3CCD camera (Dage-MTI, Michigan City, IN) with a 10x macro video zoom lens (Edmund Optics, Barrington, NJ) recording video at 30 frames per second. The TEVGs were preconditioned via 15 cycles of pressurization from 0 to 150 mm Hg. Compliance measurements were made by pressurizing the sample from 0 to 250 mm Hg and was calculated as the percent change in outer diameter (D/D_0) per 100 mm Hg: $C = 1/b \times 100$, where b is the slope of a line fit to the pressure vs. D/D_0 curve between 80

and 120 mm Hg. Burst pressure measurements were made by pressurizing the samples until leakage from the TEVGs was detected. Suture retention strength measurements were made at 37°C using a Dynamic Mechanical Thermal Analyzer V (DMTA V, Rheometric Scientific, Piscataway, NJ). A loop of 6-0 Prolene suture (BV-1 needle, Ethicon Inc., Somerville, NJ) 2 mm from the edge of the TEVG, and pulled in the longitudinal direction using the DMTA at a constant rate of 4 mm/min. It should be noted that a single TEVG was sutured to the transected abdominal aorta of an already deceased Wistar rat, which had been used for a different experimental purpose (*Figure 8c*).

Statistics

Mean and standard deviation were calculated for all measurements with a minimum of at least $n = 5$ for each condition. ANOVA was used for multiple comparisons, Tukey post hoc analysis for parametric data, and Kruskal-Wallis for non-parametric data. Values of $p < 0.05$ were considered statistically significant and p values were marked with: * for $p < 0.05$, ** for $p < 0.01$, *** for $p < 0.001$, and **** for $p < 0.0001$.

Results

Collagen sheet fabrication and characterization

Here, we report the adaptation of a microfluidic strategy[55] for the rapid and continuous formation of ultrathin and handleable collagen sheets (see *Figures 1*, *2* and *Methods – Aligned collagen sheet formation and crosslinking*). Rat tail type I collagen dissolved in deionized water (pH 2) at a 5 mg/mL concentration is injected (*Figures 1a* and *2a*) into the middle of three layers of a microfluidic device (*Figures 1b, c* and *2a*) at a flow rate, *Qc*, of 400 µL/min. The microfluidic device distributes the collagen solution uniformly in the lateral direction. A flow focusing buffer (FFB, pH 8) is concurrently injected (*Figures 1a* and *2a*) into the top and bottom layers of the microfluidic device (*Figures 1b, c* and *2a*) at a flow rate, Q_B, of 4,000 µL/min. The collagen layer exiting the microfluidic device is hydrodynamically focused[132] between the top and bottom emerging layers of FFB, which also provide fluid flow-induced shear stress. As the collagen solution approaches its isoelectric point (pH 7.4)[133], hydrophobic interactions overcome the now reduced electrostatic repulsion between the positively charged collagen molecules. This results in pH-triggered fibrillogenesis, by favoring collagen fibril nucleation and the subsequent self-assembly of collagen molecules into fibrils. Fibrillar compaction is promoted by polyethylene glycol (PEG), the key component of FFB. PEG, a molecular crowding agent, creates a hypertonic environment causing the expulsion of water from the collagen layer and resulting in fibrillar compaction. The emerging collagen sheet is geometrically confined through a rectangular shaped space by the top and bottom components of constriction (labeled as [1] in *Figure 2*). Lastly, the emerging collagen sheet

is strained by a rotating mandrel, inducing fibrillar alignment along the extrusion direction, x (*Figure 1a* and *2b*). Following collagen sheet washing with deionized water and air drying, the process of fibril growth is completed with a 48 h incubation in a buffer system to promote fibrillogenesis (FPB) at 37°C[33,129].

The combined effects of hydrodynamic focusing, fluid flow-induced shear stress, pH-induced fibrillogenesis, macromolecular crowding, geometric confinement, strain and evaporative drying produce ultrathin and handleable collagen sheets (*Figure 2b*). The properties of the obtained sheets were quantified as a function of the dimensionless velocity, $V^* = (V_P - V_T)/V_T$, where V_P is the mandrel velocity and $V_T = (Q_B + Q_C)/(W_0 H_C)$ is the total bulk velocity of the solutions passing through flow constriction. The value of V_T remained unchanged in this study, by keeping constant the FFB (Q_B = 4,000 µL/min) and collagen (Q_C = 400 µL/min) flow rates, width of the microfluidic device exit section (W_0 = 35 mm) and height of constriction (H_C = 1 mm) (*Figure 1*). Consequently, V^* in our studies varied only with changing mandrel speeds, V_P = 2.3 – 23 mm/s, and hence was as an indirect measure of the amount of strain exerted on the extruded collagen sheet pictured in *Figures 2b* and *3a*.

Aspects of both the macro- and microstructure of the extruded collagen sheets were investigated in this study. With regards to the macrostructure of the collagen sheets, increasing V^* from 0.1 to 10 resulted in decreasing sheet thickness, δ, from 5.2 ± 0.9 µm to 1.9 ± 0.3 µm (*Figure 3b*). Similarly, increasing V^* resulted in sheet width decreasing from the width of the microfluidic device exit section, W_0 = 35 mm, to 12.0 ± 0.2 mm at V^* = 10. Data on the microstructure of the collagen sheets is included in *Figure 4*. TEM

was used to investigate collagen fibril structure, compaction and alignment. *Figure 4a* includes TEM images of collagen sheet samples in the (*y*-*z*) and (*x*-*z*) planes for $V^* = 0.6$, 4.5, and 10. Average fibril diameter remained unchanged at 35.1 ± 0.1 nm for $V^* = 0.6$, 4.5, and 10 (*Figure 4b*). Visual examination of the TEM images (*Figure 4a*) reveals an evident increase in both fibrillar compaction and alignment with increasing V^*. Quantitative analysis of the TEM images agrees with this qualitative assessment. More specifically, fibril packing density increases from 141 ± 46 to 470 ± 61 fibrils/μm^2 for $V^* = 0.6$ and 10, respectively (*Figure 4c*). Fast Fourier Transform of TEM images in the (*x*-*z*) plane illustrated an increase in fibrillar alignment in the direction of the mandrel-exerted strain (x-direction) with increasing V^*.

The biostability of the aligned and compacted collagen sheets was called into question with the incidental observation of their complete dissolution within a week of incubation in PBS at 37°C (data not shown). This posed a significant challenge to the use of these collagen sheets for the subsequent generation of a TEVG. Hence, to quantify and address this phenomenon, an acid solubility test (see *Methods – Aligned collagen sheet formation and crosslinking*) was carried out. Collagen sheets ($V^* = 10$) treated with the cytocompatible crosslinking agent, genipin[134,135] had a lower extractable percentage than untreated sheets (5.5 ± 2.0% vs 98.7 ± 0.6%) and similar to that of the commonly used crosslinking agent, glutaraldehyde (5.6 ± 1.9%) (*Figure 5a*). Thus, genipin crosslinking was a viable solution to enhancing the *in vitro* biostability of the collagen sheets.

Having established the biostability of genipin-crosslinked collagen sheets, their mechanical properties, including the elastic modulus (E), ultimate tensile strength (UTS)

and strain-to-failure, were characterized. For increasing V^* values of 0.6, 4.5 and 10, the elastic modulus and UTS increased, while strain-to-failure decreased (*Figure 5b-d*). More specifically, the elastic modulus was 6.5 ± 0.6, 20.1 ± 2.6 and 38.3 ± 3.7 MPa for V^* = 0.6, 4.5 and 10, respectively. The UTS was 1.3 ± 0.5, 2.7 ±0.5 and 5.2 ± 0.6 MPa for V^* = 0.6, 4.5 and 10, respectively. Lastly, the strain-to-failure was 20.7 ± 2.6, 13.5 ± 2.3 and 12.4 ± 3.5 MPa for V^* = 0.6, 4.5 and 10, respectively. The thickness of genipin crosslinked collagen sheets (V^* = 10) was calculated at 1.7 ± 0.2 µm (*Figure 5e*) and was not statistically different from that of non-crosslinked sheets (1.9 ± 0.3 µm, *Figure 3b*). Two and three collagen sheets were sequentially stacked on top of each other to generate bilamellar and trilamellar structures respectively. The significance of these multilamellar structures becomes evident in the next section describing TEVG fabrication. Regardless, bilamellar and trilamellar collagen sheets (V^* = 10) had thicknesses of 3.3 ± 0.3 µm and 4.8 ± 0.4 µm, respectively (*Figure 5e*). These values were lower than would be expected by the theoretical sequential addition of single layers (1.7 ± 0.2 µm, *Figure 5e*).

TEVG fabrication and characterization

A flowchart of the 13-day long experimental process employed to generate the TEVGs is summarized in *Figure 6a* and detailed in the *Methods* section. In brief, days 1 to 3 consist of collagen sheet extrusion, incubation in FPB for 48 h and genipin crosslinking. Having previously established that higher mandrel velocities (i.e. higher V^* values) yielded collagen sheets with increased compaction (*Figure 4c*), alignment (*Figure 4d*) and tensile strength (*Figure 5b, c*), only V* = 10 collagen sheets were used for TEVG fabrication. Days

3 to 6 consist of collagen sheet seeding with HAoSMCs, incubation in full media for 72 hours and rolling with the use of a custom-made setup comprised of a conveyor belt and rolling mandrel (*Figure 6b*). Lastly, days 6 to 13 consist of a 7-day incubation of the TEVGs in full medium supplemented with ascorbic acid. The structural and mechanical properties of these constructs was in turn investigated.

Hematoxylin and eosin staining of cross-sections of the TEVG and rat abdominal aorta (*Figure 7a-d*) allow for qualitative comparisons between their corresponding microstructures. Aside from the tunica adventitia present in the rat aorta alone (*Figure 7a*), the TEVG recapitulates the native arterial wall microstructure. As seen in *Figures 7b* and *d*, the end result of the TEVG fabrication process is a tubular structure composed of circumferential HAoSMC layers (with intact cellular viability, data not shown) alternating with layers of compact, aligned and crosslinked collagen fibrils. The TEVG depicted (*Figure 7b, d*) was generated with the use of trilamellar collagen sheets. The wall thickness of TEVGs was 61.5 ± 4, 130.5 ± 9.1 and 232.7 ± 31.7 μm for single, bilamellar and trilamellar constructs, respectively (*Figure 7e*). In comparison, the rat abdominal aorta wall thickness ranged from 173 ± 21 μm in 120 g rats to 375 ± 91 μm in 300 g rats.

The burst pressure and suture retention strength of TEVGs increased with the increasing number of collagen sheets stacked in each collagen layer (*Figure 8a, b*). Single and bilamellar TEVGs had burst pressure and SRS averages of 226.5 ± 124.7 mm Hg, 3.7 ±1.3 gF and 1,483.3 ± 262.8 mm Hg, 66.5 ± 21.2 gF, respectively. Trilamellar constructs yielded the maximum burst pressure of 2,645 ± 346 mm Hg and SRS of 153.5 ± 37.4 gF. However, the TEVGs exhibited poor compliance with values less than 1%/mm Hg (data

not shown), regardless of lamellar composition. A single and successful attempt was made to suture a trilamellar-based TEVG to the transected abdominal aorta of an already deceased rat and is depicted in *Figure 8c*.

Discussion

Collagen sheet fabrication and characterization

In this study, we reported the use of a microfluidic strategy[55] for rapid and continuous formation of ultrathin, handleable, aligned and compacted collagen sheets. This novel fabrication process allowed for the alteration of collagen sheet properties in a controlled fashion by varying the strain exerted by the rotating mandrel (meaning V_P and hence V^*). The tunable properties of fabricated collagen sheets included, thickness (*Figure 3b*), width (*Figure 3c*), fibril compaction (*Figure 4c*) and alignment (*Figure 4d*), and tensile strength (*Figure 5b-d*). This fabrication strategy affords significant control over and achieves better levels of fibrillar compaction and alignment compared to the traditional collagen biomaterial fabrication methods of casting, bioprinting and fiber spinning[15].

This was likely achieved by combining different, published approaches for controlling fibrillar formation, compaction and alignment. Approaches and principles included in the present fabrication method were straining[42] provided by the rotating mandrel, geometric confinement[43,44] provided by the constriction device, macromolecular crowding[136,137] provided by the PEG component of FFB and lastly fluid flow-induced shear stress[45,46,47], hydrodynamic focusing[132] and pH neutralization provided by the FFB flow above and below the collagen layer (*Figures 1* and *2*). Individually, these approaches have exhibited only limited control over collagen fibrillar alignment and compaction and only in one-dimensional or substrate-attached two-dimensional structures. Their combined effect in the present fabrication process allowed for the generation of highly aligned and compacted (*Figures 4c, d*), multidimensional collagen structures in a tunable and scalable

manner suitable for the engineering of collagen-based tissues, such as tendons, corneas, skin and blood vessels. For the purposes of vascular graft engineering specifically, the resulting collagen fibril diameters of 35.1 ± 0.1 nm were independent of *V** (*Figure 4b*) and fell within the 30 – 100 nm range observed in collagen fibrils of native vascular walls[61].

One limitation of this fabrication process was the limited *in vitro* biostability of the collagen sheets determined by the incidental observation of their complete dissolution within a week of incubation in PBS at 37°C (data not shown). This was due to the absence of interfibrillar covalent bonds or crosslinks, endogenously created by enzymes like lysyl oxidase[9]. This limitation was overcome with the use of the crosslinking agent genipin, acting on lysine, hydroxylysine and arginine residues of collagen[134,135]. Genipin-crosslinked collagen sheets exhibited greater biostability, as suggested by a percentage extractable values in an acid solubility test on par with that of glutaraldehyde-treated sheets (*Figure 5a*). A main advantage of genipin over traditional crosslinking agents, such as formaldehyde and glutaraldehyde, is its cytocompatible nature[134]. Consequently, the resulting crosslinked and hence biostable collagen sheets were suitable for the purposes of tissue engineering.

TEVG fabrication and characterization

The 13-day long TEVG fabrication process summarized in *Figure 6a* yielded tubular structures composed of circumferential HAoSMC layers alternating with layers of compact, aligned and crosslinked collagen fibrils (*Figure 7b, d*). Importantly, H&E staining of cross-sections of the TEVG revealed a qualitatively strong resemblance to the native arterial wall

microstructure when compared to rat abdominal aorta (*Figure 7a-d*). However, the tunica intima and adventitia present in endogenous blood vessels[56] (*Figure 7a*) was absent from our TEVG, since it was an attempt to recapitulate the microstructure of the tunica media alone. Yet, the obtained TEVG recapitulated native arterial wall microstructure more closely than previously reported tissue engineering approaches[69,80,107]. At the same time, the wall thickness of trilamellar TEVGs, 232.7 ± 31.7 µm (*Figure 7e*), was within the wall thickness range of samples of rat abdominal aorta (173 ± 21 µm to 375 ± 91 µm for 120 and 300 g rats, respectively). Moving forward this will be important for implanting our TEVG into an animal model and investigating its *in vivo* performance.

The maximum burst pressure and SRS averages were both reached by trilamellar TEVGs measuring 2,645 ± 346 mm Hg and 153.5 ± 37.4 gF, respectively (*Figure 8a, b*). As a reminder, bi- and trilamellar TEVGs were obtained by spreading two and three collagen sheets sequentially on top of each other (stacking) prior to crosslinking and cell-seeding (see *Methods - Aligned collagen sheet formation and crosslinking*). Collagen is abundant in native vascular walls[56] and contributes to their tensile stiffness[56,60] and their resulting ability to tolerate physiologic changes in blood pressure and flow[65,66]. Consequently, it is to be expected that adding more collagen to the TEVG wall, in the form of sequentially stacked collagen sheets, results in superior mechanical properties (*Figure 8a, b*). Importantly, the single yet successful attempt to suture a trilamellar TEVG to a transected rat abdominal aorta (*Figure 8c*) illustrated that the aforementioned SRS range translates to an ability to suture the graft to native tissue. This fact will facilitate any subsequent *in vivo* investigations of these TEVGs.

The trilamellar TEVG burst pressure average is on par with the burst pressure ranges of both native human veins and arteries, namely 1,600 – 2,500 and 2,200 – 4,225 mm Hg for saphenous veins[68,69,70,71] and popliteal arteries[68,69], respectively. The TEVG SRS average is also on par with the SRS ranges of both native human veins and arteries, namely 88 – 200 and 180 – 250 gF for internal thoracic arteries[70,72] and umbilical veins[69,70,71], respectively. These mechanical congruencies offer some support for our original hypothesis that recapitulating the native vessel wall microstructure will also afford TEVGs with comparable mechanical properties.

The trilamellar TEVG burst pressure and SRS averages were also comparable or superior to some of the best examples of TEVGs previously published. For example, the L'Heureux group using the scaffold-free sheet-based tissue engineering approach reported TEVGs with burst pressure and SRS ranges of 3,000 – 4,000 mm Hg and 140 – 180 gF, respectively[70]. Among scaffold-based approaches, decellularized porcine carotid artery-derived grafts yielded burst pressure ranges of 1,000 – 2,000 mm Hg and a SRS of 300 gF[93]. With the use of a polyglycolic acid scaffold-based TEVG, the Niklason group reported burst pressure and SRS ranges of 1,000 – 2,000 mm Hg and 40 – 50 gF, respectively[106]. Compared to these examples, the present TEVG was able to achieve comparable mechanical properties without the use of synthetic or composite biomaterials[106] and without prolonged bioreactor incubation times[70,93,106] that can reach up to 28 weeks[78]. In contrast, our shorter, 13-day long fabrication process provides a more cost-effective and scalable solution.

However, our tissue engineering approach also has some important limitations. Firstly, a number of the fabrication steps were manual, rendering parts of the process susceptible to error depending on the experimenter's manual dexterity. Among these steps, spreading of collagen sheets on glass slides and removal of the rolling mandrels (*Figure 6a*) could introduce defects to the constructs limiting the yield and scalability of the fabrication process. Secondly, the resulting TEVGs exhibited poor compliance (<1%/mm Hg) regardless of lamellar composition (data not shown). The reason for the resulting poor compliance is likely two-fold. Collagen fibrils in human aorta and saphenous vein are circumferentially aligned at angles of 18.8° – 58.9°[2] and 2° – 83°[64], respectively. The absence of angles between alternating collagen layers in our TEVG could party explain its low compliance. Concurrently and possibly more importantly, collagen alone was used to fabricate the biopolymer-based scaffold, which lacked elastin. Elastin significantly contributes to the elastic properties of blood vessels allowing for their elastic deformation in response to pulsatile blood flow[56,60]. Regardless of the approach, improving the TEVGs' compliance will be crucial moving forward, since *in vivo* neointimal hyperplasia and ensuing graft stenosis have been attributed to a compliance mismatch between vascular grafts and native blood vessels[67].

Future work

There is still a significant amount of investigation that has to be performed prior to the present TEVG approach being suitable for *in vivo* studies in animal models and humans. Among others, the introduction of an internal layer of endothelial cells and improving the

graft's *in vitro* compliance will be key aspects of future work. With regards to graft endothelialization, the innermost lining of native vascular walls, the tunica intima, is composed of a non-thrombogenic monolayer of endothelial cells[56]. Endothelial cells inhibit platelet activation and prevent thrombus formation by secreting molecules like nitric oxide[56]. An inner layer of endothelial cells has been included in some[70,84,102], but not other TEVG fabrication methods[82,106]. Regardless, endothelialization of our TEVG will be important to reduce its thrombogenicity post-implantation in future animal models.

The poor compliance of the present TEVGs will also have to be addressed in future experiments either through the introduction of angles between alternating collagen layers or of elastin or both. The custom-made rolling setup (*Figure 6b*) for the transformation of planar, cell-seeded collagen sheets into tubular constructs can be altered to achieve the former. More specifically, a stepper motor can be introduced for the rolling mandrel to translate perpendicularly to the collagen sheet and the rolling direction. Such a setup is currently under investigation in our lab for the creation of an angle between alternating collagen layers. The incorporation of elastin into the fabrication process will be more challenging. Approaches could include the adaptation of the existing microfluidic setup for the generation of elastin sheets and their subsequent incorporation into the TEVG. Alternatively, established fabrication processes like fiber spinning could be investigated for the introduction of elastin into the construct.

Lastly, future experiments will inevitably have to include testing in an animal model. Despite promising *in vitro* mechanical properties, previous TEVG attempts have faced challenges post-implantation in humans and animal models including graft

aneurysmal dilation and thrombosis [79,97], post-implantation neointimal hyperplasia[84] and poor long-term patency rates[98,112]. It is yet to be determined whether our TEVG approach will overcome these challenges faced by other researchers.

Conclusion

In this study we reported the use of a microfluidic strategy for rapid and continuous formation of ultrathin, handleable and highly aligned and compacted collagen sheets with tunable properties including thickness, width, compaction, alignment and tensile strength. These constructs were in turn used to fabricate TEVGs yielding tubular structures composed of circumferential HAoSMC layers alternating with layers of compact, aligned and crosslinked collagen fibrils. The resulting TEVG recapitulated both the microstructure and some of the mechanical properties (burst pressure, suture retention) of native arteries. Importantly, the present TEVG approach achieved *in vitro* mechanical properties comparable to previous attempts without the use of synthetic or composite biomaterials and without prolonged bioreactor incubation times, hence being a more cost-effective and scalable solution. Challenges however remain, given the TEVGs' poor compliance and the need for an inner layer of endothelial cells. Future efforts should concentrate on these limitations in preparation for the graft's eventual implantation into animal models.

Tables and Figures

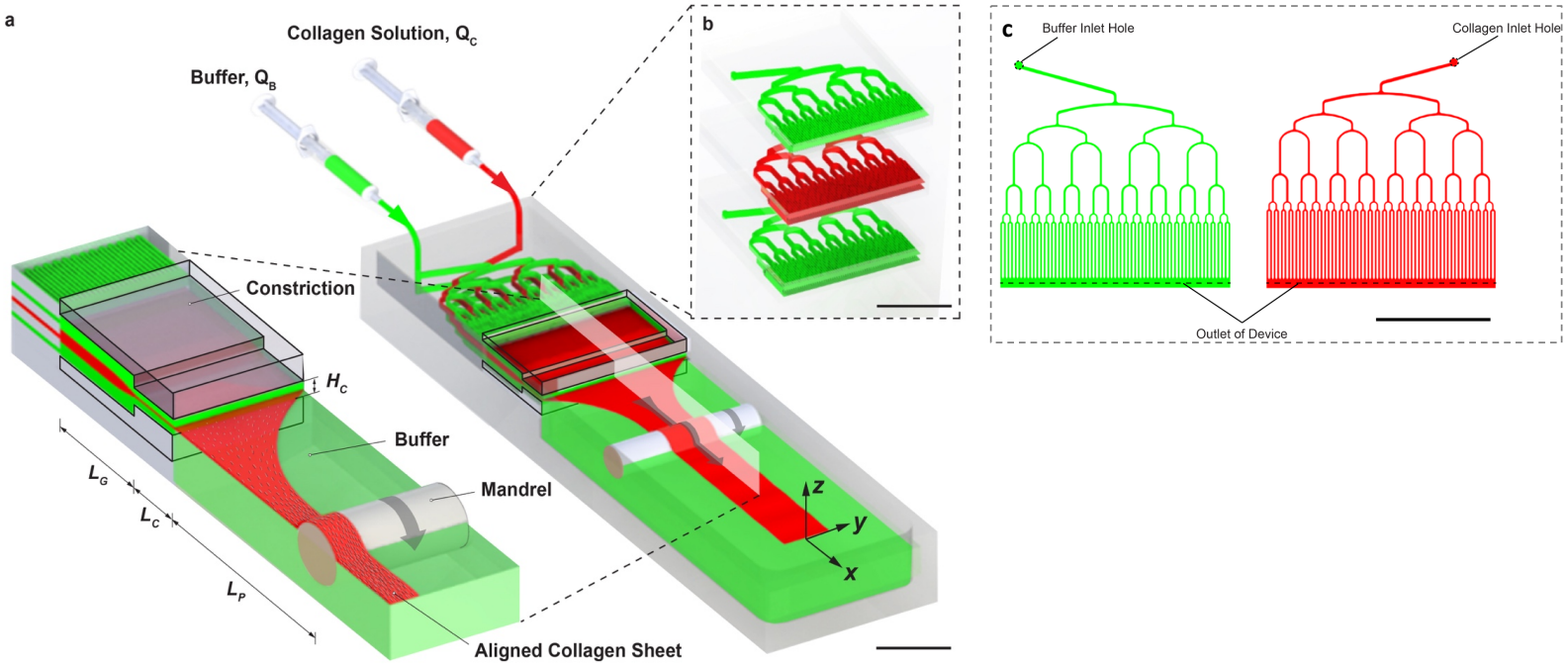

Figure 1. First rendering of experimental setup. A schematic illustration of the microfluidic device used to generate aligned collagen sheets (designed by collaborators). Flow focusing buffer (FFB) solution (pH 8, green color) and collagen solution (pH 2, red color) are delivered to the three layers of the microfluidic device as depicted, with fibril formation induced by the pH differential. The collagen sheet generated at the device exit is hydrodynamically focused between the top and bottom buffer solutions and guided through geometric constriction. The emerging collagen sheet undergoes fibrillogenesis. The strain on the sheet induced by passing over a rotating mandrel (diameter D = 12.7 mm, velocity V_p) promotes fibrillar alignment. Continued incubation in the buffer solution post-straining, washing and drying result in 230 mm-long collagen sheets. **(a)** An enlarged view of the microfluidic system used to generate aligned collagen sheets (L_G = 2 mm, L_C = 7.6 mm, L_P = 55 mm, H_C = 1 mm). **(b)** Schematic illustration of three-layered microfluidic device with hierarchical microchannel networks used for sheet formation (W_0 = 35 mm). **(c)** Design of the FFB (left; top and bottom layers) and collagen (right; middle layer) solution microfluidic device layers. The device is cut along the dashed line to expose the microfluidic channels. Scale bar **(a, b)** 10 mm **(c)** 17.5 mm.

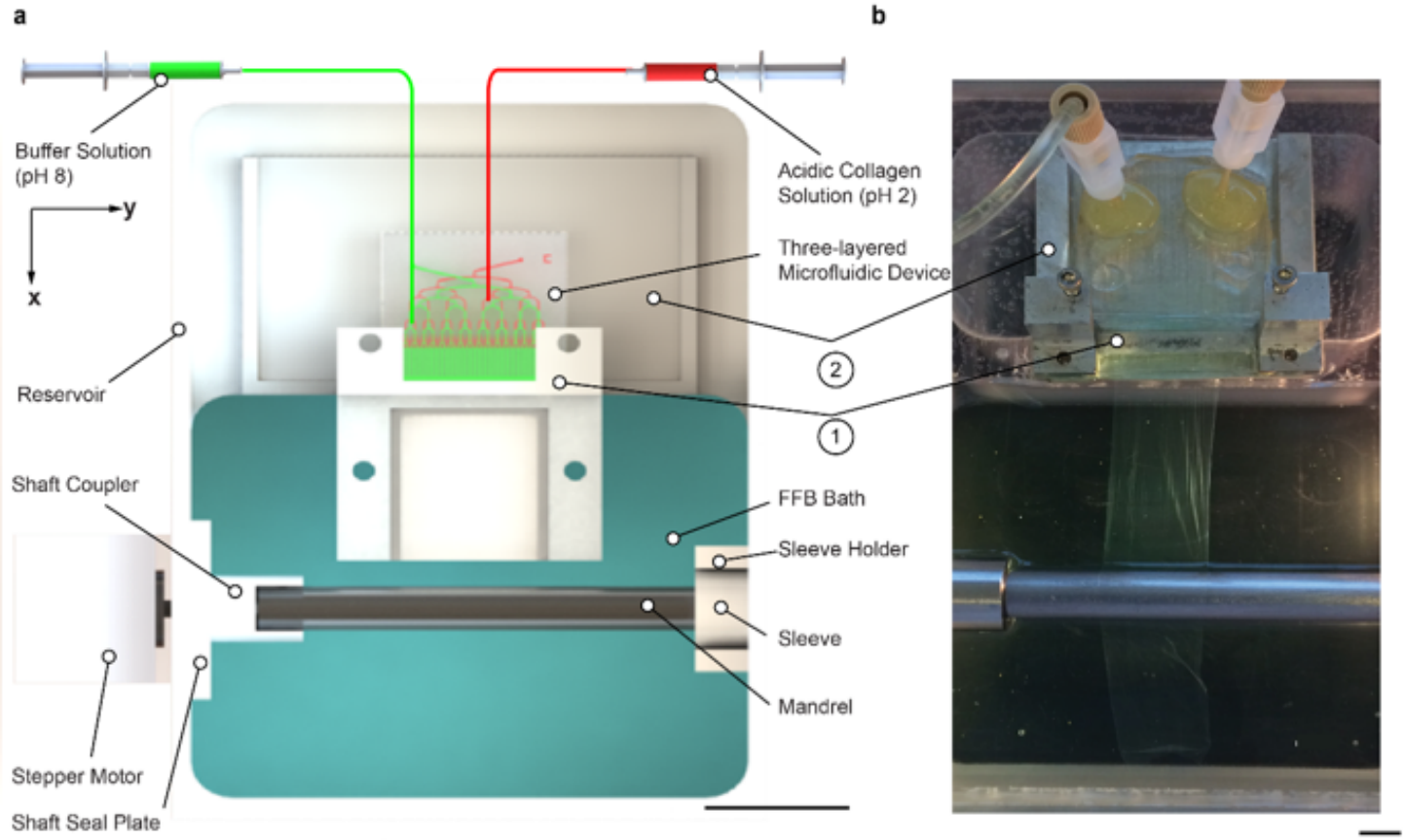

Figure 2. Second rendering of experimental setup. (a) Rendered image of experimental setup used for the generation of aligned collagen sheets (designed by collaborators). The FFB (pH 8, green color) and collagen solutions (pH 2, red color) are depicted entering the microfluidic device. Here (1) and (2) represent respectively the top and bottom pieces of the constrictor which provides geometric constriction for the emerging collagen sheet. The rotating mandrel straining the emerging collagen sheet is also depicted. Post-straining, the extruded collagen sheet is incubated in the FFB bath, before washing and drying. **(b)** Photograph of aligned collagen sheet emerging from constriction bracket submerged in the FFB bath and eventually passing over the rotating mandrel. Scale bars **(a)** 35 mm, **(b)** 20 mm.

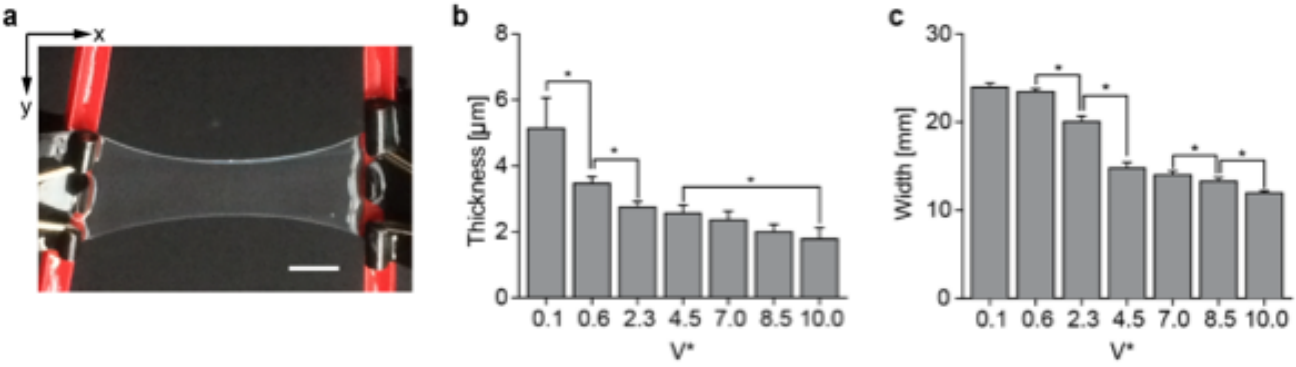

Figure 3. Macrostructure of aligned collagen sheets. (a) Photograph of a collagen sheet ($V^* = 4.5$) supported on both ends. **(b)** Sheet thickness, δ, after extrusion and post-processing for different values of $V^* = \frac{V_P W_0 H_C}{(Q_B + Q_C)} - 1$. Smallest thickness, 1.9 µm ± 0.3 µm, for highly aligned sheets ($V^* = 10$). **(c)** Straining during extrusion by the rotating mandrel reduced sheet width with increasing V^*. Smallest value of 12 mm at $V^* = 10$. Scale bar **(a)** 10 mm.

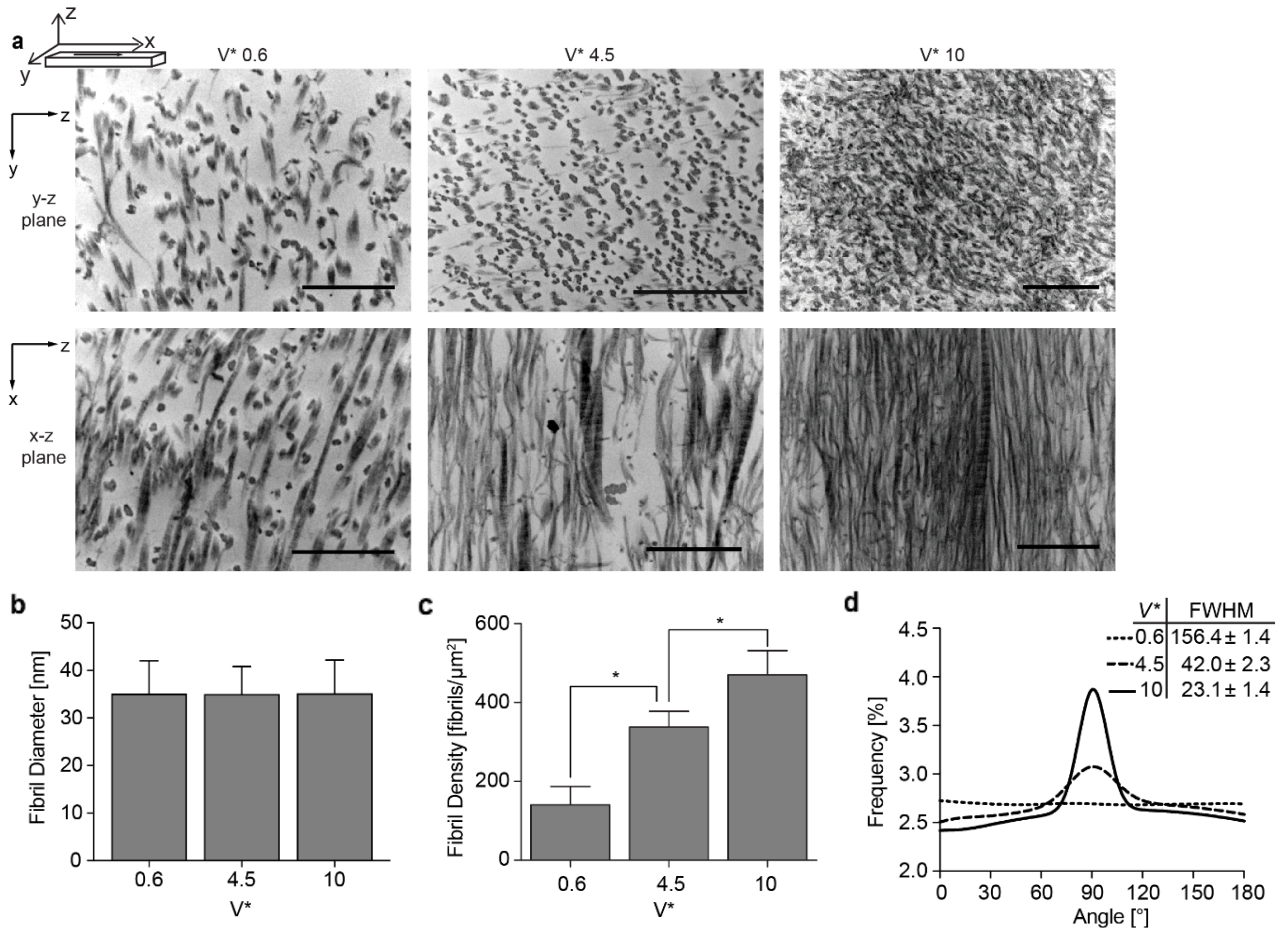

Figure 4. Microstructure of aligned collagen sheets. Data contributed by collaborators. **(a)** Transmission electron microscope (TEM) images at $V^* = 0.6$, 4.5, and 10 for assessment of collagen fibrillar alignment and compaction. As V^* increases from 0.6 to 4.5 to 10, **(b)** mean fibril diameter remains constant at 35 nm, **(c)** fibril density (number of fibrils/µm^2) increases, **(d)** fibrillar alignment increases as suggested by angular fibrillar alignment with full width at half maximum (FWHM) decreasing from 156.4 nm to 23.1 nm. Scale bar **(a)** 500 nm.

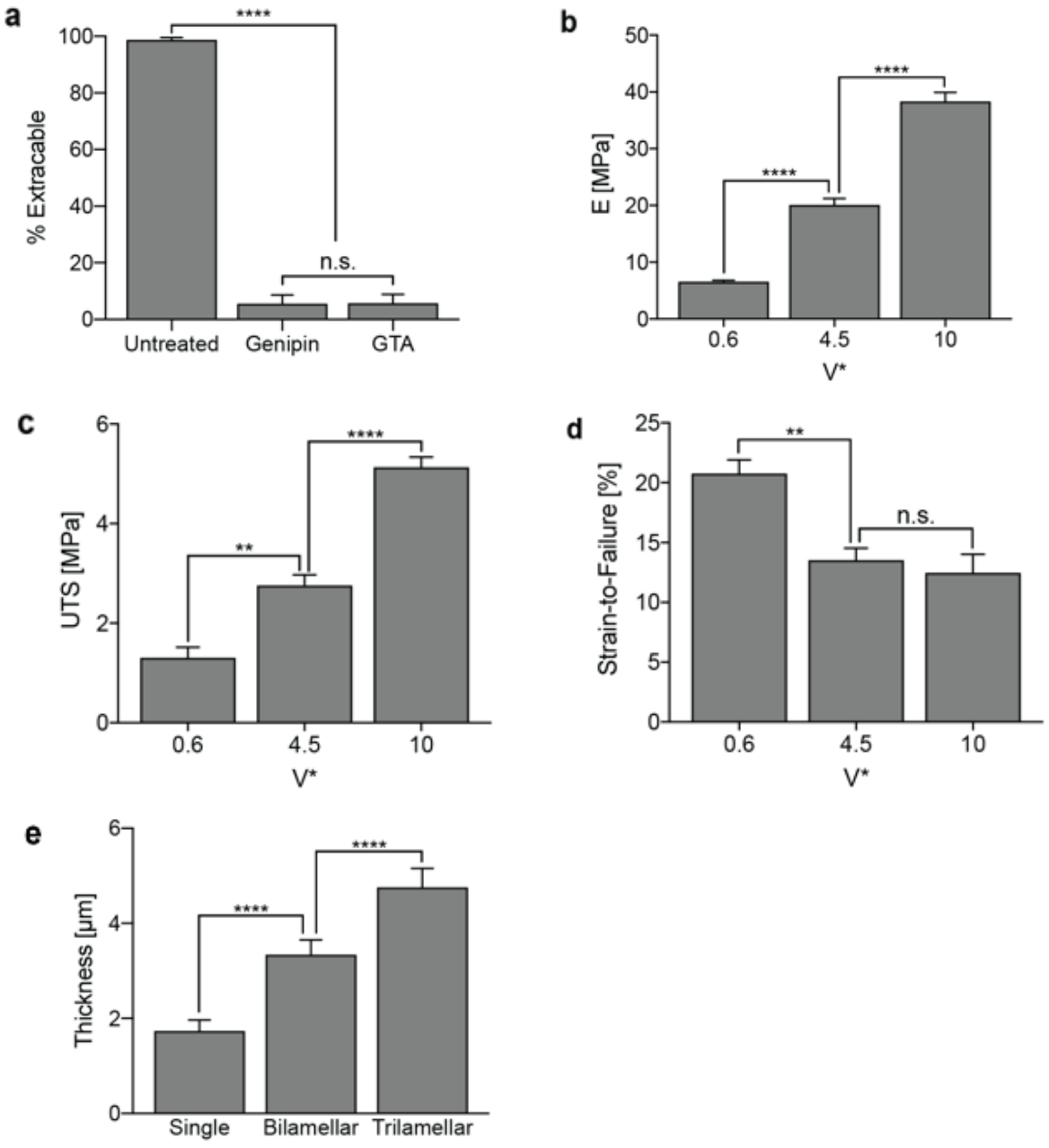

Figure 5. Structural and mechanical properties of crosslinked, aligned collagen sheets. **(a)** The percent extractable was evaluated for untreated and genipin (6 mg/mL) treated collagen sheets and compared to glutaraldehyde (1%) treated sheets serving as a positive control. Genipin crosslinking increased the biostability of the aligned collagen sheets. Increasing *V** in crosslinked sheets resulted in **(b)** an increased elastic modulus, **(c)** and ultimate tensile strength (UTS) along with **(d)** a decrease in strain-to-failure. **(e)** Thickness is compared for single, bilamellar and trilamellar stacked crosslinked sheets. A non-linear increase is observed when stacking aligned collagen sheets.

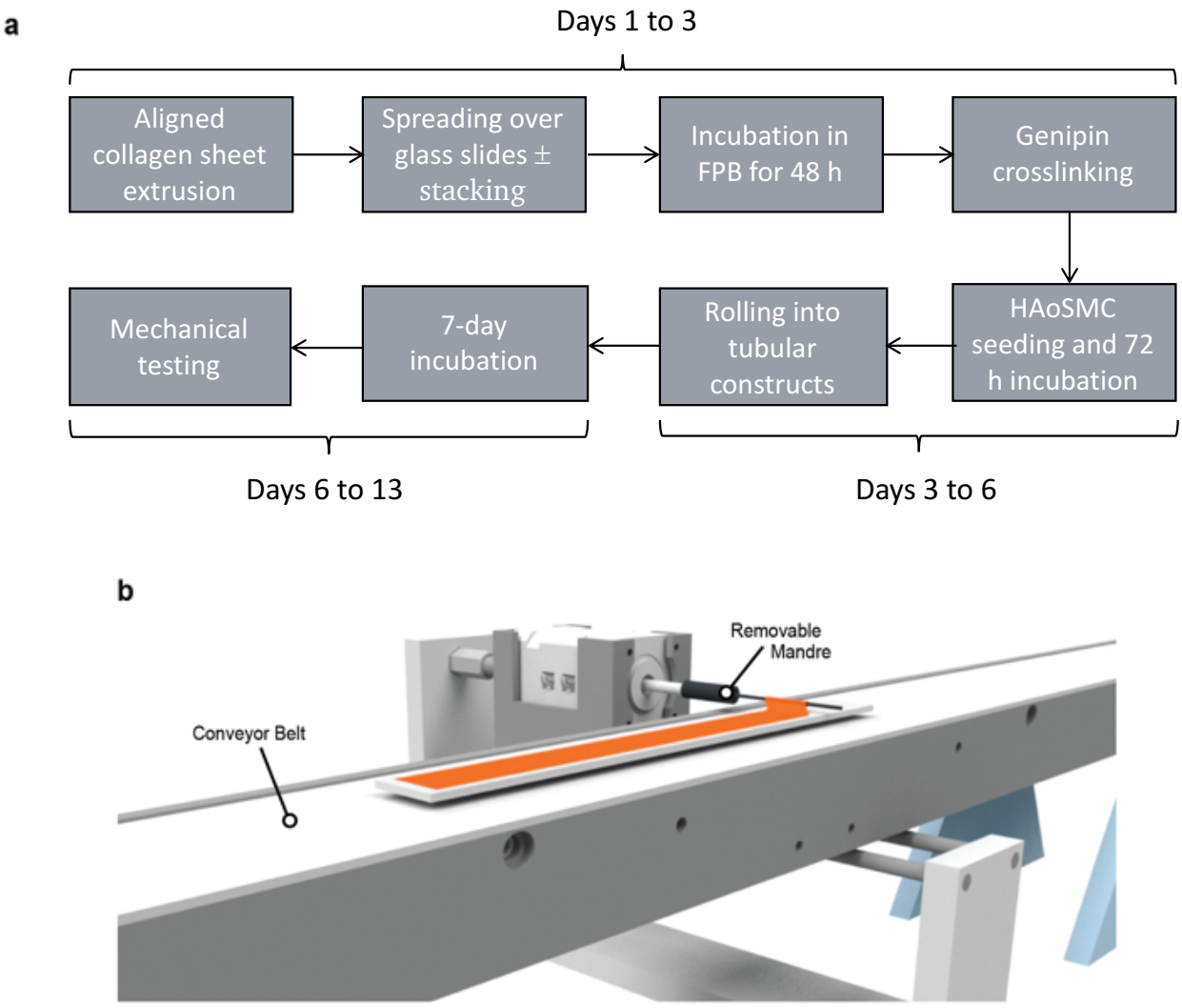

Figure 6. TEVG generation protocol. (a) A flowchart of the experimental steps from aligned collagen sheet extrusion to the generation of a TEVG. **(b)** Cell-seeded, crosslinked collagen sheets (L = 23 cm, W = 1.5 cm) were fabricated into tubular constructs by rolling around removable mandrels (Φ = 1.5 mm) using a custom-built setup consisting of a conveyor belt and rolling domain. A rendered image (designed by collaborators) of the custom-built setup is depicted.

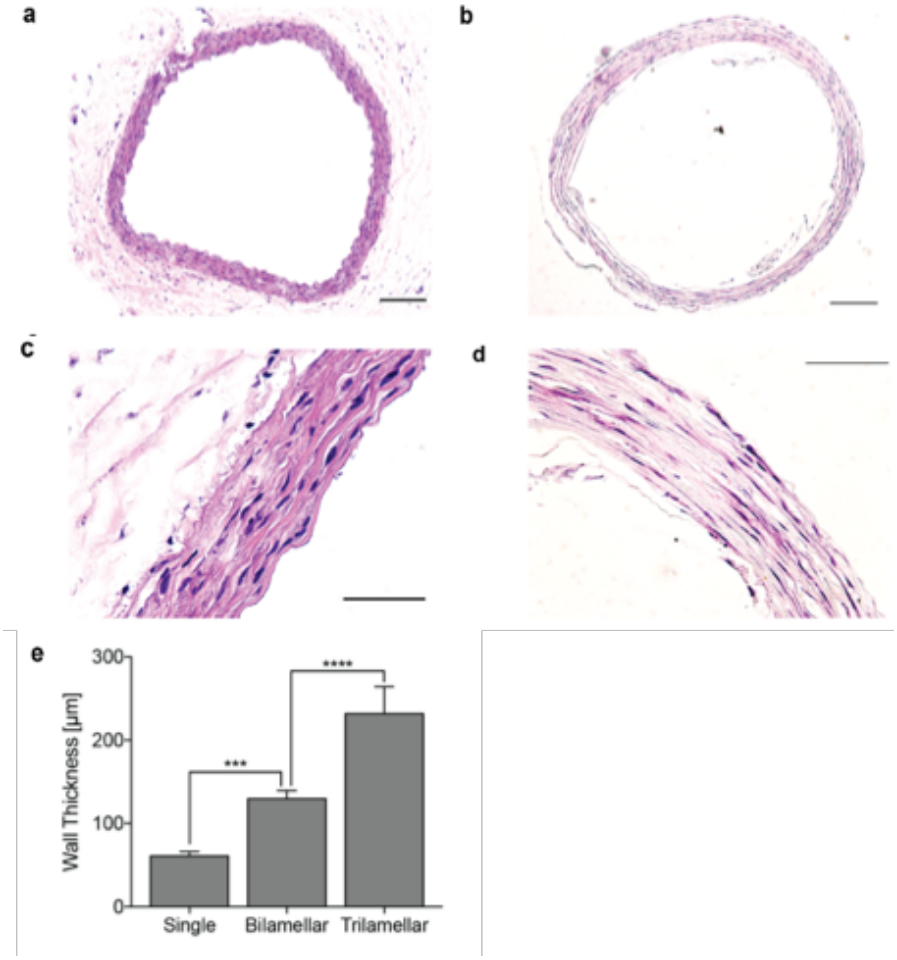

Figure 7. Structural characterization of TEVGs. Hematoxylin and eosin stained cross-sections of **(a, c)** abdominal aorta of a 300 g rat and **(b, d)** engineered, trilamellar TEVGs showing the TEVGs recapitulating the native arterial wall microstructure. **(e)** Crosslinked collagen sheet stacking yielded TEVGs with wall thickness ranging from 61.5 ± 4 to 232.7 ± 31.7 µm for single and trilamellar constructs, respectively. Scale bars **(a, b)** 500 µm and **(c, d)** 200 µm.

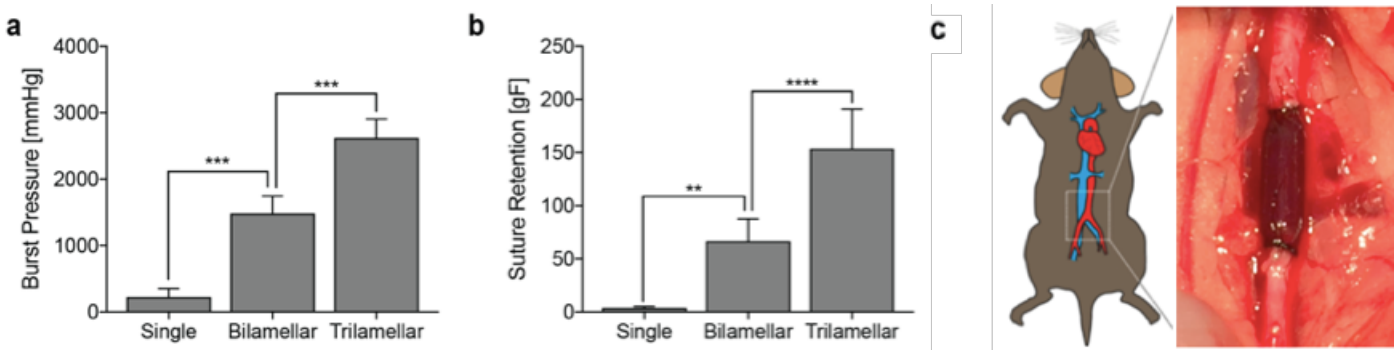

Figure 8. Mechanical characterization of TEVGs. Crosslinked collagen sheet stacking yielded TEVGs with **(a)** increasing burst pressure averages with a maximum of 2,645 ± 346 mm Hg and **(b)** increasing suture retention strength averages with a maximum of 153.5 ± 37.4 gF in trilamellar constructs. **(c)** End-to-end anastomosis of trilamellar-based TEVG in infrarenal rat aorta to illustrate the ability to suture the construct to endogenous vessels.

References

[1]Linsenmayer, T. F. “Collagen.” *Cell Biology of Extracellular Matrix*, by Elizabeth D. Hay, Plenum Press, 1991, pp. 7–44.

[2]P. Fratzl, in *Collagen: Structure and Mechanics*, (Ed: P. Fratzl), Springer US, Boston, MA 2008, 1.

[3]Mithieux SM, Weiss AS. Elastin. *Adv Protein Chem*. 2005;70:437-61. Review. PubMed PMID: 15837523.

[4]Von der Mark, K. “Chapter 1 - Structure, Biosynthesis and Gene Regulation of Collagens in Cartilage and Bone.” *Dynamics of Bone and Cartilage Metabolism: Principles and Clinical Applications*, by Markus J. Seibel et al., Academic Press, 2006, pp. 3–40.

[5]Mayne R, Brewton RG. New members of the collagen superfamily. *Curr Opin Cell Biol*. 1993 Oct; 5(5): 883-90. Review. PubMed PMID: 8240831.

[6]Parenteau-Bareil R, Gauvin R, Berthod F. Collagen-Based Biomaterials for Tissue Engineering Applications. *Materials (Basel)*. 2010 Mar 16;3(3):1863–1887. doi: 10.3390/ma3031863. PMCID: PMC5445871.

[7]Olsen, B. R. “Collagen Biosynthesis.” *Cell Biology of Extracellular Matrix*; by Elizabeth D. Hay, Plenum Press, 1991, pp. 177−220.

[8]Ricard-Blum S. The collagen family. *Cold Spring Harb Perspect Biol*. 2011 Jan 1;3(1):a004978. doi: 10.1101/cshperspect.a004978. Review. PubMed PMID: 21421911; PubMed Central PMCID: PMC3003457.

[9]Stenzel KH, Miyata T, Rubin AL. Collagen as a biomaterial. *Annu Rev Biophys Bioeng*. 1974;3(0):231-53. Review. PubMed PMID: 4607533.

[10]Gelse K, Pöschl E, Aigner T. Collagens--structure, function, and biosynthesis. *Adv Drug Deliv Rev*. 2003 Nov 28;55(12):1531-46. Review. PubMed PMID: 14623400.

[11]Miller A, Wray JS. Molecular packing in collagen. *Nature*. 1971 Apr 16;230(5294):437-9. PubMed PMID: 4929973.

[12]Ottani V, Raspanti M, Ruggeri A. Collagen structure and functional implications. *Micron*. 2001 Apr;32(3):251-60. Review. PubMed PMID: 11006505.

[13]Annabi N, Mithieux SM, Camci-Unal G, Dokmeci MR, Weiss AS, Khademhosseini A. Elastomeric Recombinant Protein-based Biomaterials. *Biochem Eng J*. 2013 Aug 15;77:110-118. doi: 10.1016/j.bej.2013.05.006. PMID: 23935392; PMCID: PMC3735178.

[14]Friess W. Collagen--biomaterial for drug delivery. *Eur J Pharm Biopharm*. 1998 Mar;45(2):113-36. Review. PubMed PMID: 9704909.

[15]David Miranda-Nieves and Elliot L. Chaikof. Collagen and Elastin Biomaterials for the Fabrication of Engineered Living Tissues. *ACS Biomaterials Science & Engineering* **2017** *3* (5), 694-711 doi: 10.1021/acsbiomaterials.6b00250

[16]Browne S, Zeugolis DI, Pandit A. Collagen: finding a solution for the source. *Tissue Eng Part A*. 2013 Jul;19(13-14):1491-4. doi: 10.1089/ten.TEA.2012.0721. Epub 2013 Jan 21. PubMed PMID: 23240852; PubMed Central PMCID: PMC3665299.

[17]Pacak CA, Powers JM, Cowan DB. Ultrarapid purification of collagen type I for tissue engineering applications. *Tissue Eng Part C Methods*. 2011 Sep;17(9):879-85. doi: 10.1089/ten.TEC.2010.0720. Epub 2011 Jun 1. PubMed PMID: 21486201; PubMed Central PMCID: PMC3162468.

[18]Gallop, P. M.; Seifter, S. Preparation and properties of soluble collagens. *Methods Enzymol*. 1963, 6, 635−641.

[19]Setina CM, Haase JP, Glatz CE. Process integration for recovery of recombinant collagen type I α1 from corn seed. *Biotechnol Prog*. 2016 Jan-Feb;32(1):98-107. doi: 10.1002/btpr.2191. Epub 2015 Nov 17. PubMed PMID: 26518757.

[20]Buechter DD, Paolella DN, Leslie BS, Brown MS, Mehos KA, Gruskin EA. Co-translational incorporation of trans-4-hydroxyproline into recombinant proteins in bacteria. *J Biol Chem*. 2003 Jan 3;278(1):645-50. Epub 2002 Oct 23. PubMed PMID: 12399455.

[21]Willard JJ, Drexler JW, Das A, Roy S, Shilo S, Shoseyov O, Powell HM. Plant-derived human collagen scaffolds for skin tissue engineering. *Tissue Eng Part A*. 2013 Jul;19(13-14):1507-18. doi:

10.1089/ten.TEA.2012.0338. Epub 2013 Feb 19. PubMed PMID: 23298216; PubMed Central PMCID: PMC3665310.

[22]Rutschmann C, Baumann S, Cabalzar J, Luther KB, Hennet T. Recombinant expression of hydroxylated human collagen in Escherichia coli. *Appl Microbiol Biotechnol*. 2014 May;98(10):4445-55. doi: 10.1007/s00253-013-5447-z. Epub 2013 Dec 21. PubMed PMID: 24362857.

[23]Yaari A, Posen Y, Shoseyov O. Liquid crystalline human recombinant collagen: the challenge and the opportunity. *Tissue Eng Part A*. 2013 Jul;19(13-14):1502-6. doi: 10.1089/ten.tea.2012.0335. Epub 2013 Jan 31. PubMed PMID: 23368756.

[24]Kariduraganavar, M. Y.; Kittur, A. A.; Kamble, R. R. *Polymer Synthesis and Processing*, 1st ed.; Elsevier Inc.: New York, 2014.

[25]Lee CH, Singla A, Lee Y. Biomedical applications of collagen. *Int J Pharm*. 2001 Jun 19;221(1-2):1-22. Review. PubMed PMID: 11397563.

[26]Guo B, Sun Y, Finne-Wistrand A, Mustafa K, Albertsson AC. Electroactive porous tubular scaffolds with degradability and non-cytotoxicity for neural tissue regeneration. *Acta Biomater*. 2012 Jan;8(1):144-53. doi: 10.1016/j.actbio.2011.09.027. Epub 2011 Sep 28. PubMed PMID: 21985870.

[27]Weinberg CB, Bell E. A blood vessel model constructed from collagen and cultured vascular cells. *Science*. 1986 Jan 24;231(4736):397-400. PubMed PMID: 2934816.

[28]Inzana JA, Olvera D, Fuller SM, Kelly JP, Graeve OA, Schwarz EM, Kates SL, Awad HA. 3D printing of composite calcium phosphate and collagen scaffolds for bone regeneration. *Biomaterials*. 2014 Apr;35(13):4026-34. doi: 10.1016/j.biomaterials.2014.01.064. Epub 2014 Feb 14. PubMed PMID: 24529628; PubMed Central PMCID: PMC4065717.

[29]Lee W, Debasitis JC, Lee VK, Lee JH, Fischer K, Edminster K, Park JK, Yoo SS. Multi-layered culture of human skin fibroblasts and keratinocytes through three-dimensional freeform fabrication. *Biomaterials*. 2009 Mar;30(8):1587-95. doi: 10.1016/j.biomaterials.2008.12.009. Epub 2008 Dec 23. PubMed PMID: 19108884.

[30]Yanez M, Rincon J, Dones A, De Maria C, Gonzales R, Boland T. In vivo assessment of printed microvasculature in a bilayer skin graft to treat full-thickness wounds. *Tissue Eng Part A*. 2015 Jan;21(1-2):224-33. doi: 10.1089/ten.TEA.2013.0561. Epub 2014 Sep 3. PubMed PMID: 25051339; PubMed Central PMCID: PMC4293098.

[31]Michael S, Sorg H, Peck CT, Koch L, Deiwick A, Chichkov B, Vogt PM, Reimers K. Tissue engineered skin substitutes created by laser-assisted bioprinting form skin-like structures in the dorsal skin fold chamber in mice. *PLoS One*. 2013;8(3):e57741. doi: 10.1371/journal.pone.0057741. Epub 2013 Mar 4. PubMed PMID: 23469227; PubMed Central PMCID: PMC3587634.

[32]Guillotin B, Souquet A, Catros S, Duocastella M, Pippenger B, Bellance S, Bareille R, Rémy M, Bordenave L, Amédée J, Guillemot F. Laser assisted bioprinting of engineered tissue with high cell density and microscale organization. *Biomaterials*. 2010 Oct;31(28):7250-6. doi: 10.1016/j.biomaterials.2010.05.055. Epub 2010 Jul 2. PubMed PMID: 20580082.

[33]Caves JM, Cui W, Wen J, Kumar VA, Haller CA, Chaikof EL. Elastin-like protein matrix reinforced with collagen microfibers for soft tissue repair. *Biomaterials*. 2011 Aug;32(23):5371-9. doi: 10.1016/j.biomaterials.2011.04.009. Epub 2011 May 6. PubMed PMID: 21550111; PubMed Central PMCID: PMC3207740.

[34]Caves JM, Kumar VA, Martinez AW, Kim J, Ripberger CM, Haller CA, Chaikof EL. The use of microfiber composites of elastin-like protein matrix reinforced with synthetic collagen in the design of vascular grafts. *Biomaterials*. 2010 Sep;31(27):7175-82. doi: 10.1016/j.biomaterials.2010.05.014. Epub 2010 Jun 26. PubMed PMID: 20584549; PubMed Central PMCID: PMC3849028.

[35]Huang L, Nagapudi K, Apkarian RP, Chaikof EL. Engineered collagen-PEO nanofibers and fabrics. J Biomater Sci Polym Ed. 2001;12(9):979-93. PubMed PMID: 11787524.

[36]Huang, L.; McMillan, R. A.; Apkarian, R. P.; Pourdeyhimi, B.; Conticello, V. P.; Chaikof, E. L. Generation of Synthetic Elastin- Mimetic Small Diameter Fibers and Fiber Networks. *Macromolecules* 2000, 33 (8), 2989−2997. Doi: 10.1021/ma991858f

[37]Li WJ, Laurencin CT, Caterson EJ, Tuan RS, Ko FK. Electrospun nanofibrous structure: a novel scaffold for tissue engineering. *J Biomed Mater Res*. 2002 Jun 15;60(4):613-21. PubMed PMID: 11948520.

[38]Powell HM, Supp DM, Boyce ST. Influence of electrospun collagen on wound contraction of engineered skin substitutes. *Biomaterials*. 2008 Mar;29(7):834-43. Epub 2007 Dec 3. PubMed PMID: 18054074.

[39]Sell SA, McClure MJ, Garg K, Wolfe PS, Bowlin GL. Electrospinning of collagen/biopolymers for regenerative medicine and cardiovascular tissue engineering. *Adv Drug Deliv Rev*. 2009 Oct 5;61(12):1007-19. doi: 10.1016/j.addr.2009.07.012. Epub 2009 Aug 3. Review. PubMed PMID: 19651166.

[40]Huang C, Chen R, Ke Q, Morsi Y, Zhang K, Mo X. Electrospun collagen-chitosan-TPU nanofibrous scaffolds for tissue engineered tubular grafts. *Colloids Surf B Biointerfaces*. 2011 Feb 1;82(2):307-15. doi: 10.1016/j.colsurfb.2010.09.002. Epub 2010 Sep 15. PubMed PMID: 20888196.

[41]Zhong S, Teo WE, Zhu X, Beuerman RW, Ramakrishna S, Yung LY. An aligned nanofibrous collagen scaffold by electrospinning and its effects on in vitro fibroblast culture. *J Biomed Mater Res A*. 2006 Dec 1;79(3):456-63. PubMed PMID: 16752400.

[42]Thomopoulos S, Fomovsky GM, Holmes JW. The development of structural and mechanical anisotropy in fibroblast populated collagen gels. *J Biomech Eng*. 2005 Oct;127(5):742-50. PubMed PMID: 16248303.

[43]Saeidi N, Sander EA, Zareian R, Ruberti JW. Production of highly aligned collagen lamellae by combining shear force and thin film confinement. *Acta Biomater*. 2011 Jun;7(6):2437-47. doi: 10.1016/j.actbio.2011.02.038. Epub 2011 Mar 21. PMID: 21362500; PMCID: PMC3712118.

[44]Saeidi N, Karmelek KP, Paten JA, Zareian R, DiMasi E, Ruberti JW. Molecular crowding of collagen: a pathway to produce highly-organized collagenous structures. *Biomaterials*. 2012 Oct;33(30):7366-74. doi: 10.1016/j.biomaterials.2012.06.041. Epub 2012 Jul 29. PubMed PMID: 22846420; PubMed Central PMCID: PMC3757096.

[45]Saeidi N, Sander EA, Ruberti JW. Dynamic shear-influenced collagen self-assembly. *Biomaterials*. 2009 Dec;30(34):6581-92. doi: 10.1016/j.biomaterials.2009.07.070. Epub 2009 Sep 17. PubMed PMID: 19765820; PubMed Central PMCID: PMC3299540.

[46]Håkansson KM, Fall AB, Lundell F, Yu S, Krywka C, Roth SV, Santoro G, Kvick M, Prahl Wittberg L, Wågberg L, Söderberg LD. Hydrodynamic alignment and assembly of nanofibrils resulting in strong cellulose filaments. *Nat Commun*. 2014 Jun 2;5:4018. doi: 10.1038/ncomms5018. PubMed PMID: 24887005; PubMed Central PMCID: PMC4059937.

[47]Lanfer B, Freudenberg U, Zimmermann R, Stamov D, Körber V, Werner C. Aligned fibrillar collagen matrices obtained by shear flow deposition. *Biomaterials*. 2008 Oct;29(28):3888-95. doi: 10.1016/j.biomaterials.2008.06.016. Epub 2008 Jul 7. PubMed PMID: 18606448.

[48]Cheng X, Gurkan UA, Dehen CJ, Tate MP, Hillhouse HW, Simpson GJ, Akkus O. An electrochemical fabrication process for the assembly of anisotropically oriented collagen bundles. *Biomaterials*. 2008 Aug;29(22):3278-88. doi: 10.1016/j.biomaterials.2008.04.028. Epub 2008 May 9. PubMed PMID: 18472155.

[49]Zhang S, Liu X, Barreto-Ortiz SF, Yu Y, Ginn BP, DeSantis NA, Hutton DL, Grayson WL, Cui FZ, Korgel BA, Gerecht S, Mao HQ. Creating polymer hydrogel microfibres with internal alignment via electrical and mechanical stretching. *Biomaterials*. 2014 Mar;35(10):3243-51. doi: 10.1016/j.biomaterials.2013.12.081. Epub 2014 Jan 15. PubMed PMID: 24439410; PubMed Central PMCID: PMC3923323.

[50]Xu B, Chow M-J, Zhang Y. Experimental and modeling study of collagen scaffolds with the effects of crosslinking and fiber alignment. *International journal of biomaterials*. 2011. https://doi.org/10.1155/2011/172389

[51]Torbet J, Malbouyres M, Builles N, Justin V, Roulet M, Damour O, Oldberg A, Ruggiero F, Hulmes DJ. Orthogonal scaffold of magnetically aligned collagen lamellae for corneal stroma reconstruction. *Biomaterials*. 2007 Oct;28(29):4268-76. Epub 2007 Jul 5. PubMed PMID: 17618680.

[52]Guo C, Kaufman LJ. Flow and magnetic field induced collagen alignment. *Biomaterials*. 2007 Feb;28(6):1105-14. Epub 2006 Nov 16. PubMed PMID: 17112582.

[53]Lanfer B, Hermann A, Kirsch M, Freudenberg U, Reuner U, Werner C, Storch A. Directed growth of adult human white matter stem cell-derived neurons on aligned fibrillar collagen. *Tissue Eng Part A*. 2010 Apr;16(4):1103-13. doi: 10.1089/ten.TEA.2009.0282. PubMed PMID: 19860550.

[54]Lee P, Lin R, Moon J, Lee LP. Microfluidic alignment of collagen fibers for in vitro cell culture. *Biomed Microdevices*. 2006 Feb;8, 35-41, doi:10.1007/s10544-006-6380-z.

[55]Leng L, McAllister A, Zhang B, Radisic M, Günther A. Mosaic hydrogels: one-step formation of multiscale soft materials. Adv Mater. 2012 Jul 17;24(27):3650-8. doi: 10.1002/adma.201201442. Epub 2012 Jun 20. PubMed PMID: 22714644.

[56]Patel A, Fine B, Sandig M, Mequanint K. Elastin biosynthesis: The missing link in tissue-engineered blood vessels. *Cardiovasc Res*. 2006 Jul 1;71(1):40-9. Epub 2006 Feb 28. Review. PubMed PMID: 16566911.

[57]Hilenski LL, Griendling KK. "Vascular Smooth Muscle." *Vascular Medicine: A Companion to Braunwald's Heart Disease*. 2013. 25–42. doi:10.1016/b978-1-4377-2930-6.00003-3

[58]Kielty CM, Sherratt MJ, Shuttleworth CA. Elastic fibres. *J Cell Sci*. 2002 Jul 15;115(Pt 14):2817-28. Review. PubMed PMID: 12082143.

[59]D'Armiento J. Decreased elastin in vessel walls puts the pressure on. *J Clin Invest*. 2003 Nov;112(9):1308-10. PubMed PMID: 14597755; PubMed Central PMCID: PMC228487.

[60]Ratcliffe A. Tissue engineering of vascular grafts. *Matrix Biol*. 2000 Aug;19(4):353-7. Review. PubMed PMID: 10963996.

[61]Merrilees MJ, Tiang KM, Scott L. Changes in collagen fibril diameters across artery walls including a correlation with glycosaminoglycan content. *Connect Tissue Res*. 1987;16(3):237-57. PubMed PMID: 2956051.

[62]Montes GS. Structural biology of the fibres of the collagenous and elastic systems. *Cell Biol Int*. 1996 Jan;20(1):15-27. Review. PubMed PMID: 8936403.

[63]Dahl SL, Rhim C, Song YC, Niklason LE. Mechanical properties and compositions of tissue engineered and native arteries. *Ann Biomed Eng*. 2007 Mar;35(3):348-55. Epub 2007 Jan 6. PubMed PMID: 17206488; PubMed Central PMCID: PMC2605789.

[64]Canham PB, Finlay HM, Boughner DR. Contrasting structure of the saphenous vein and internal mammary artery used as coronary bypass vessels. *Cardiovasc Res*. 1997 Jun;34(3):557-67. PubMed PMID: 9231039.

[65]Wagenseil JE, Mecham RP. Vascular extracellular matrix and arterial mechanics. *Physiol Rev*. 2009 Jul;89(3):957-89. doi: 10.1152/physrev.00041.2008. Review. PubMed PMID: 19584318; PubMed Central PMCID: PMC2775470.

[66]Shadwick RE. Mechanical design in arteries. *J Exp Biol*. 1999 Dec;202(Pt 23):3305-13. Review. PubMed PMID: 10562513.

[67]Kumar VA, Brewster LP, Caves JM, Chaikof EL. Tissue Engineering of Blood Vessels: Functional Requirements, Progress, and Future Challenges. *Cardiovasc Eng Technol*. 2011 Sep 1;2(3):137-148. PubMed PMID: 23181145

[68]Wise SG, Byrom MJ, Waterhouse A, Bannon PG, Weiss AS, Ng MK. A multilayered synthetic human elastin/polycaprolactone hybrid vascular graft with tailored mechanical properties. *Acta Biomater*. 2011 Jan;7(1):295-303. doi: 10.1016/j.actbio.2010.07.022. Epub 2010 Jul 23. Erratum in: Acta Biomater. 2011 Mat;7(3):1429. PubMed PMID: 20656079.

[69]Dahl SL, Kypson AP, Lawson JH, Blum JL, Strader JT, Li Y, Manson RJ, Tente WE, DiBernardo L, Hensley MT, Carter R, Williams TP, Prichard HL, Dey MS, Begelman KG, Niklason LE. Readily available tissue-engineered vascular grafts. *Sci Transl Med*. 2011 Feb 2;3(68):68ra9. doi: 10.1126/scitranslmed.3001426. PubMed PMID: 21289273.

[70]L'Heureux N, Dusserre N, Konig G, Victor B, Keire P, Wight TN, Chronos NA, Kyles AE, Gregory CR, Hoyt G, Robbins RC, McAllister TN. Human tissue-engineered blood vessels for adult arterial revascularization. *Nat Med*. 2006 Mar;12(3):361-5. Epub 2006 Feb 19. PubMed PMID: 16491087; PubMed Central PMCID:PMC1513140.

[71]Schaner PJ, Martin ND, Tulenko TN, Shapiro IM, Tarola NA, Leichter RF, Carabasi RA, Dimuzio PJ. Decellularized vein as a potential scaffold for vascular tissue engineering. *J Vasc Surg*. 2004 Jul;40(1):146-53. PubMed PMID: 15218475.

[72]Konig G, McAllister TN, Dusserre N, Garrido SA, Iyican C, Marini A, Fiorillo A, Avila H, Wystrychowski W, Zagalski K, Maruszewski M, Jones AL, Cierpka L, de la Fuente LM, L'Heureux N. Mechanical properties of completely autologous human tissue engineered blood vessels compared to human saphenous vein and mammary artery. *Biomaterials*. 2009 Mar;30(8):1542-50. doi: 10.1016/j.biomaterials.2008.11.011. Epub 2008 Dec 25. PubMed PMID: 19111338; PubMed Central PMCID: PMC2758094.

[73]Shaw JA, Kingwell BA, Walton AS, Cameron JD, Pillay P, Gatzka CD, Dart AM. Determinants of coronary artery compliance in subjects with and without angiographic coronary artery disease. *J Am Coll Cardiol*. 2002 May 15;39(10):1637-43. PubMed PMID: 12020491.

[74]van Andel CJ, Pistecky PV, Borst C. Mechanical properties of porcine and human arteries: implications for coronary anastomotic connectors. *Ann Thorac Surg*. 2003 Jul;76(1):58-64; discussion 64-5. PubMed PMID: 12842513.

[75]Tai NR, Giudiceandrea A, Salacinski HJ, Seifalian AM, Hamilton G. In vivo femoropopliteal arterial wall compliance in subjects with and without lower limb vascular disease. *J Vasc Surg*. 1999 Nov;30(5):936-45. PubMed PMID: 10550193.

[76]Chen J, Alexander GC, Bobba PS, Jun HW. Recent Progress in Vascular Tissue-Engineered Blood Vessels. *Adv Exp Med Biol*. 2018;1064:123-144. doi:10.1007/978-981-13-0445-3_8. Review. PubMed PMID: 30471030.

[77]Ong CS, Zhou X, Huang CY, Fukunishi T, Zhang H, Hibino N. Tissue engineered vascular grafts: current state of the field. *Expert Rev Med Devices*. 2017 May;14(5):383-392. doi: 10.1080/17434440.2017.1324293. Epub 2017 May 9. Review. PubMed PMID: 28447487.

[78]L'Heureux N, Pâquet S, Labbé R, Germain L, Auger FA. A completely biological tissue engineered human blood vessel. *FASEB J*. 1998 Jan;12(1):47-56. PubMed PMID: 9438410.

[79]McAllister TN, Maruszewski M, Garrido SA, Wystrychowski W, Dusserre N, Marini A, Zagalski K, Fiorillo A, Avila H, Manglano X, Antonelli J, Kocher A, Zembala M, Cierpka L, de la Fuente LM, L'heureux N. Effectiveness of haemodialysis access with an autologous tissue-engineered vascular graft: a multicenter cohort study. *Lancet*. 2009 Apr 25;373(9673):1440-6. doi: 10.1016/S0140-6736(09)60248-8. PubMed PMID: 19394535.

[80]Wystrychowski W, McAllister TN, Zagalski K, Dusserre N, Cierpka L, L'Heureux N. First human use of an allogeneic tissue-engineered vascular graft for hemodialysis access. *J Vasc Surg*. 2014 Nov;60(5):1353-1357. doi:10.1016/j.jvs.2013.08.018. Epub 2013 Oct 5. PubMed PMID: 24103406.

[81]Jung Y, Ji H, Chen Z, Fai Chan H, Atchison L, Klitzman B, Truskey G, Leong KW. Scaffold-free, Human Mesenchymal Stem Cell-Based Tissue Engineered Blood Vessels. *Sci Rep*. 2015 Oct 12;5:15116. doi: 10.1038/srep15116. PubMed PMID: 26456074; PubMed Central PMCID: PMC4600980.

[82]Yokoyama U, Tonooka Y, Koretake R, Akimoto T, Gonda Y, Saito J, Umemura M, Fujita T, Sakuma S, Arai F, Kaneko M, Ishikawa Y. Arterial graft with elastic layer structure grown from cells. *Sci Rep*. 2017 Mar 10;7(1):140. doi: 10.1038/s41598-017-00237-1. PubMed PMID: 28273941; PubMed Central PMCID: PMC5428065.

[83]Itoh M, Nakayama K, Noguchi R, Kamohara K, Furukawa K, Uchihashi K, Toda S, Oyama J, Node K, Morita S. Scaffold-Free Tubular Tissues Created by a Bio-3D Printer Undergo Remodeling and Endothelialization when Implanted in Rat Aortae. *PLoS One*. 2015 Sep 1;10(9):e0136681.doi:10.1371/journal.pone.0136681. eCollection 2015. Erratum in: PLoS One. 2015;10(12):e0145971. PubMed PMID: 26325298; PubMed Central PMCID: PMC4556622.

[84]Gui L, Muto A, Chan SA, Breuer CK, Niklason LE. Development of decellularized human umbilical arteries as small-diameter vascular grafts. *Tissue Eng Part A*. 2009 Sep;15(9):2665-76. doi: 10.1089/ten.TEA.2008.0526. PubMed PMID: 19207043; PubMed Central PMCID: PMC2735599.

[85]Cho SW, Lim SH, Kim IK, Hong YS, Kim SS, Yoo KJ, Park HY, Jang Y, Chang BC, Choi CY, Hwang KC, Kim BS. Small-diameter blood vessels engineered with bone marrow-derived cells. *Ann Surg*. 2005 Mar;241(3):506-15. PubMed PMID: 15729075; PubMed Central PMCID: PMC1356991.

[86] Zhou M, Liu Z, Wei Z, Liu C, Qiao T, Ran F, Bai Y, Jiang X, Ding Y. Development and validation of small-diameter vascular tissue from a decellularized scaffold coated with heparin and vascular endothelial growth factor. *Artif Organs*. 2009 Mar;33(3):230-9. doi:10.1111/j.1525-1594.2009.00713.x. PubMed PMID: 19245522.

[87] Narita Y, Kagami H, Matsunuma H, Murase Y, Ueda M, Ueda Y. Decellularized ureter for tissue-engineered small-caliber vascular graft. *J Artif Organs*. 2008;11(2):91-9. doi: 10.1007/s10047-008-0407-6. Epub 2008 Jul 6. PubMed PMID: 18604613.

[88]Zhou M, Liu Z, Li K, Qiao W, Jiang X, Ran F, Qiao T, Liu C. Beneficial effects of granulocyte-colony stimulating factor on small-diameter heparin immobilized decellularized vascular graft. *J Biomed Mater Res A*. 2010 Nov;95(2):600-10. doi: 10.1002/jbm.a.32864. PubMed PMID: 20725964.

[89]Fitzpatrick JC, Clark PM, Capaldi FM. Effect of decellularization protocol on the mechanical behavior of porcine descending aorta. *Int J Biomater*. 2010;2010. pii: 620503. doi: 10.1155/2010/620503. Epub 2010 Jul 4. PubMed PMID: 20689621;PubMed Central PMCID: PMC2910464.

[90] Liu GF, He ZJ, Yang DP, Han XF, Guo TF, Hao CG, Ma H, Nie CL. Decellularized aorta of fetal pigs as a potential scaffold for small diameter tissue engineered vascular graft. *Chin Med J* (Engl). 2008 Aug 5;121(15):1398-406. PubMed PMID:18959117.

[91]Simionescu DT, Lu Q, Song Y, Lee JS, Rosenbalm TN, Kelley C, Vyavahare NR. Biocompatibility and remodeling potential of pure arterial elastin and collagen scaffolds. *Biomaterials*. 2006 Feb;27(5):702-13. Epub 2005 Jul 26. PubMed PMID:16048731.

[92]Chuang TH, Stabler C, Simionescu A, Simionescu DT. Polyphenol-stabilized tubular elastin scaffolds for tissue engineered vascular grafts. *Tissue Eng Part A*. 2009 Oct;15(10):2837-51. doi: 10.1089/ten.TEA.2008.0394. PubMed PMID:19254115; PubMed Central PMCID: PMC2792047.

[93]Conklin BS, Richter ER, Kreutziger KL, Zhong DS, Chen C. Development and evaluation of a novel decellularized vascular xenograft. *Med Eng Phys*. 2002 Apr;24(3):173-83. PubMed PMID: 12062176.

[94]Sandusky GE, Lantz GC, Badylak SF. Healing comparison of small intestine submucosa and ePTFE grafts in the canine carotid artery. *J Surg Res*. 1995 Apr;58(4):415-20. PubMed PMID: 7723321.

[95]Derham C, Yow H, Ingram J, Fisher J, Ingham E, Korrosis SA, Homer-Vanniasinkam S. Tissue engineering small-diameter vascular grafts: preparation of a biocompatible porcine ureteric scaffold. *Tissue Eng Part A*. 2008 Nov;14(11):1871-82. doi: 10.1089/ten.tea.2007.0103. PubMed PMID: 18950273.

[96]Clarke DR, Lust RM, Sun YS, Black KS, Ollerenshaw JD. Transformation of nonvascular acellular tissue matrices into durable vascular conduits. *Ann Thorac Surg*. 2001 May;71(5 Suppl):S433-6. PubMed PMID: 11388242.

[97]Sharp MA, Phillips D, Roberts I, Hands L. A cautionary case: the SynerGraft vascular prosthesis. *Eur J Vasc Endovasc Surg*. 2004 Jan;27(1):42-4. PubMed PMID: 14652835.

[98]Das N, Bratby MJ, Shrivastava V, Cornall AJ, Darby CR, Boardman P, Anthony S, Uberoi R. Results of a seven-year, single-centre experience of the long-term outcomes of bovine ureter grafts used as novel conduits for haemodialysis fistulas. *Cardiovasc Intervent Radiol*. 2011 Oct;34(5):958-63. doi: 10.1007/s00270-011-0096-z. Epub 2011 Mar 1. PubMed PMID: 21360240.

[99]Spark JI, Yeluri S, Derham C, Wong YT, Leitch D. Incomplete cellular depopulation may explain the high failure rate of bovine ureteric grafts. *Br J Surg*. 2008 May;95(5):582-5. doi: 10.1002/bjs.6052. PubMed PMID: 18344206.

[100]Soletti L, Hong Y, Guan J, Stankus JJ, El-Kurdi MS, Wagner WR, Vorp DA. A bilayered elastomeric scaffold for tissue engineering of small diameter vascular grafts. *Acta Biomater*. 2010 Jan;6(1):110-22. doi: 10.1016/j.actbio.2009.06.026. Epub 2009 Jun 18. PubMed PMID: 19540370; PubMed Central PMCID: PMC3200232.

[101]Pektok E, Nottelet B, Tille JC, Gurny R, Kalangos A, Moeller M, Walpoth BH. Degradation and healing characteristics of small-diameter poly(epsilon-caprolactone) vascular grafts in the rat systemic arterial

circulation. *Circulation*. 2008 Dec 9;118(24):2563-70. doi:10.1161/CIRCULATIONAHA.108.795732. Epub 2008 Nov 24. PubMed PMID: 19029464.

[102]Niklason LE, Gao J, Abbott WM, Hirschi KK, Houser S, Marini R, Langer R. Functional arteries grown in vitro. *Science*. 1999 Apr 16;284(5413):489-93. PubMed PMID: 10205057.

[103]Iwasaki K, Kojima K, Kodama S, Paz AC, Chambers M, Umezu M, Vacanti CA. Bioengineered three-layered robust and elastic artery using hemodynamically-equivalent pulsatile bioreactor. *Circulation*. 2008 Sep 30;118(14 Suppl):S52-7. doi: 10.1161/CIRCULATIONAHA.107.757369. PubMed PMID: 18824769.

[104]Stekelenburg M, Rutten MC, Snoeckx LH, Baaijens FP. Dynamic straining combined with fibrin gel cell seeding improves strength of tissue-engineered small-diameter vascular grafts. *Tissue Eng Part A*. 2009 May;15(5):1081-9. doi:10.1089/ten.tea.2008.0183. PubMed PMID: 18831688.

[105]Hibino N, Yi T, Duncan DR, Rathore A, Dean E, Naito Y, Dardik A, Kyriakides T, Madri J, Pober JS, Shinoka T, Breuer CK. A critical role for macrophages in neovessel formation and the development of stenosis in tissue-engineered vascular grafts. *FASEB J*. 2011 Dec;25(12):4253-63. doi: 10.1096/fj.11-186585. Epub 2011 Aug 24. PubMed PMID: 21865316; PubMed Central PMCID: PMC3236622.

[106]Quint C, Arief M, Muto A, Dardik A, Niklason LE. Allogeneic human tissue-engineered blood vessel. *J Vasc Surg*. 2012 Mar;55(3):790-8. doi: 10.1016/j.jvs.2011.07.098. Epub 2011 Nov 4. PubMed PMID: 22056286; PubMed Central PMCID: PMC3505682.

[107]Shin'oka T, Matsumura G, Hibino N, Naito Y, Watanabe M, Konuma T, Sakamoto T, Nagatsu M, Kurosawa H. Midterm clinical result of tissue-engineered vascular autografts seeded with autologous bone marrow cells. *J Thorac Cardiovasc Surg*. 2005 Jun;129(6):1330-8. PubMed PMID: 15942574.

[108]Zhang L, Zhou J, Lu Q, Wei Y, Hu S. A novel small-diameter vascular graft: in vivo behavior of biodegradable three-layered tubular scaffolds. *Biotechnol Bioeng*. 2008 Mar 1;99(4):1007-15. PubMed PMID: 17705246.

[109]He W, Ma Z, Teo WE, Dong YX, Robless PA, Lim TC, Ramakrishna S. Tubular nanofiber scaffolds for tissue engineered small-diameter vascular grafts. *J Biomed Mater Res A*. 2009 Jul;90(1):205-16. doi: 10.1002/jbm.a.32081. PubMed PMID: 18491396.

[110]Bockeria LA, Svanidze O, Kim A, Shatalov K, Makarenko V, Cox M, Carrel T. Total cavopulmonary connection with a new bioabsorbable vascular graft: First clinical experience. *J Thorac Cardiovasc Surg*. 2017 Jun;153(6):1542-1550. doi: 10.1016/j.jtcvs.2016.11.071. Epub 2017 Feb 7. Erratum in: J Thorac Cardiovasc Surg. 2018 Mar;155(3):1348-1349. PubMed PMID: 28314534.

[111]Hibino N, McGillicuddy E, Matsumura G, Ichihara Y, Naito Y, Breuer C, Shinoka T. Late-term results of tissue-engineered vascular grafts in humans. *J Thorac Cardiovasc Surg*. 2010 Feb;139(2):431-6, 436.e1-2. doi: 10.1016/j.jtcvs.2009.09.057. PubMed PMID: 20106404.

[112]Lawson JH, Glickman MH, Ilzecki M, Jakimowicz T, Jaroszynski A, Peden EK, Pilgrim AJ, Prichard HL, Guziewicz M, Przywara S, Szmidt J, Turek J, Witkiewicz W, Zapotoczny N, Zubilewicz T, Niklason LE. Bioengineered human acellular vessels for dialysis access in patients with end-stage renal disease: two phase 2 single-arm trials. *Lancet*. 2016 May 14;387(10032):2026-34. doi: 10.1016/S0140-6736(16)00557-2. PubMed PMID: 27203778; PubMed Central PMCID: PMC4915925.

[113]Berglund JD, Nerem RM, Sambanis A. Incorporation of intact elastin scaffolds in tissue-engineered collagen-based vascular grafts. *Tissue Eng*. 2004 Sep-Oct;10(9-10):1526-35. PubMed PMID: 15588412.

[114]Buijtenhuijs P, Buttafoco L, Poot AA, Daamen WF, van Kuppevelt TH, Dijkstra PJ, de Vos RA, Sterk LM, Geelkerken BR, Feijen J, Vermes I. Tissue engineering of blood vessels: characterization of smooth-muscle cells for culturing on collagen-and-elastin-based scaffolds. *Biotechnol Appl Biochem*. 2004 Apr;39(Pt 2):141-9. PubMed PMID: 15032734.

[115]Buttafoco L, Kolkman NG, Engbers-Buijtenhuijs P, Poot AA, Dijkstra PJ, Vermes I, Feijen J. Electrospinning of collagen and elastin for tissue engineering applications. *Biomaterials*. 2006 Feb;27(5):724-34. Epub 2005 Aug 19. PubMed PMID: 16111744.

[116]Koens MJ, Faraj KA, Wismans RG, van der Vliet JA, Krasznai AG, Cuijpers VM, Jansen JA, Daamen WF, van Kuppevelt TH. Controlled fabrication of triple layered and molecularly defined collagen/elastin vascular grafts resembling the native blood vessel. *Acta Biomater*. 2010 Dec;6(12):4666-74. doi: 10.1016/j.actbio.2010.06.038. Epub 2010 Jul 7. PubMed PMID: 20619367.

[117]McClure MJ, Simpson DG, Bowlin GL. Tri-layered vascular grafts composed of polycaprolactone, elastin, collagen, and silk: Optimization of graft properties. *J Mech Behav Biomed Mater*. 2012 Jun;10:48-61. doi: 10.1016/j.jmbbm.2012.02.026. Epub 2012 Mar 14. PubMed PMID: 22520418.

[118]Lloyd-Jones D, Adams RJ, Brown TM, Carnethon M, Dai S, De Simone G, Ferguson TB, Ford E, Furie K, Gillespie C, Go A, Greenlund K, Haase N, Hailpern S, Ho PM, Howard V, Kissela B, Kittner S, Lackland D, Lisabeth L, Marelli A, McDermott MM, Meigs J, Mozaffarian D, Mussolino M, Nichol G, Roger VL, Rosamond W, Sacco R, Sorlie P, Stafford R, Thom T, Wasserthiel-Smoller S, Wong ND, Wylie-Rosett J; American Heart Association Statistics Committee and Stroke Statistics Subcommittee. Executive summary: heart disease and stroke statistics—2010 update: a report from the American Heart Association. *Circulation*. 2010 Feb 23;121(7):948-54. doi: 10.1161/CIRCULATIONAHA.109.192666. Erratum in: Circulation. 2010 Mar 30;121(12):e259. PubMed PMID: 20177011.

[119]Selvin E, Erlinger TP. Prevalence of and risk factors for peripheral arterial disease in the United States: results from the National Health and Nutrition Examination Survey, 1999-2000. *Circulation*. 2004 Aug 10;110(6):738-43. Epub 2004 Jul 19. PubMed PMID: 15262830.

[120]Andras A, Ferket B. Screening for peripheral arterial disease. *Cochrane Database Syst Rev*. 2014 Apr 7;(4):CD010835. doi: 10.1002/14651858.CD010835.pub2. Review. PubMed PMID: 24711093.

[121]Hiatt WR, Hoag S, Hamman RF. Effect of diagnostic criteria on the prevalence of peripheral arterial disease. The San Luis Valley Diabetes Study. Circulation. 1995 Mar 1;91(5):1472-9. PubMed PMID: 7867189.

[122]Criqui MH, Fronek A, Barrett-Connor E, Klauber MR, Gabriel S, Goodman D. The prevalence of peripheral arterial disease in a defined population. *Circulation*. 1985 Mar;71(3):510-5. PubMed PMID: 3156006.

[123]Heald CL, Fowkes FG, Murray GD, Price JF; Ankle Brachial Index Collaboration. Risk of mortality and cardiovascular disease associated with the ankle-brachial index: Systematic review. *Atherosclerosis*. 2006 Nov;189(1):61-9. Epub 2006 Apr 18. Review. PubMed PMID: 16620828.

[124]Conte MS, Bandyk DF, Clowes AW, Moneta GL, Seely L, Lorenz TJ, Namini H, Hamdan AD, Roddy SP, Belkin M, Berceli SA, DeMasi RJ, Samson RH, Berman SS; PREVENT III Investigators. Results of PREVENT III: a multicenter, randomized trial of edifoligide for the prevention of vein graft failure in lower extremity bypass surgery. *J Vasc Surg*. 2006 Apr;43(4):742-751; discussion 751. PubMed PMID: 16616230.

[125]Taylor LM Jr, Edwards JM, Porter JM. Present status of reversed vein bypass grafting: five-year results of a modern series. *J Vasc Surg*. 1990 Feb;11(2):193-205; discussion 205-6. PubMed PMID: 2299743.

[126]Conte MS, Belkin M, Upchurch GR, Mannick JA, Whittemore AD, Donaldson MC. Impact of increasing comorbidity on infrainguinal reconstruction: a 20-year perspective. *Ann Surg*. 2001 Mar;233(3):445-52. doi: 10.1097/00000658-200103000-00021. PMID: 11224635; PMCID: PMC1421261.

[127]Mehta RH, Ferguson TB, Lopes RD, Hafley GE, Mack MJ, Kouchoukos NT, Gibson CM, Harrington RA, Califf RM, Peterson ED, Alexander JH; Project of Ex-vivo Vein Graft Engineering via Transfection (PREVENT) IV Investigators. Saphenous vein grafts with multiple versus single distal targets in patients undergoing coronary artery bypass surgery: one-year graft failure and five-year outcomes from the Project of Ex-Vivo Vein Graft Engineering via Transfection (PREVENT) IV trial. *Circulation*. 2011 Jul 19;124(3):280-8. doi: 10.1161/CIRCULATIONAHA.110.991299. Epub 2011 Jun 27. PubMed PMID: 21709060; PubMed Central PMCID: PMC5144829.

[128]Silver FH, Trelstad RL. Type I collagen in solution. Structure and properties of fibril fragments. *J Biol Chem*. 1980 Oct 10;255(19):9427-33. PubMed PMID: 7410433.

[129]Caves JM, Kumar VA, Wen J, Cui W, Martinez A, Apkarian R, Coats JE, Berland K, Chaikof EL. Fibrillogenesis in continuously spun synthetic collagen fiber. *J Biomed Mater Res B Appl Biomater*. 2010 Apr;93(1):24-38. doi: 10.1002/jbm.b.31555. PubMed PMID: 20024969; PubMed Central PMCID: PMC3855350.

[130]Pins GD, Christiansen DL, Patel R, Silver FH. Self-assembly of collagen fibers. Influence of fibrillar alignment and decorin on mechanical properties. *Biophys J*. 1997 Oct;73(4):2164-72. PubMed PMID: 9336212; PubMed Central PMCID: PMC1181117.

[131]Kumar VA, Caves JM, Haller CA, Dai E, Liu L, Grainger S, Chaikof EL. Acellular vascular grafts generated from collagen and elastin analogs. *Acta Biomater*. 2013 Sep;9(9):8067-74. doi: 10.1016/j.actbio.2013.05.024. Epub 2013 Jun 3. PubMed PMID: 23743129; PubMed Central PMCID: PMC3733560.

[132]Knight JB, Vishwanath A, Brody JP, Austin RH. Hydrodynamic focusing on a silicon chip: mixing nanoliters in microseconds. *Physical Review Letters*. 1998, 80, 3863. https://doi.org/10.1103/PhysRevLett.80.3863

[133]Highberger JH. The isoelectric point of collagen. *J Am Chem Soc*. 1939 Sep; 61, 2302. https://doi.org/10.1021/ja01878a010

[134]Sung HW, Huang RN, Huang LL, Tsai CC, Chiu CT. Feasibility study of a natural crosslinking reagent for biological tissue fixation. *J Biomed Mater Res*. 1998 Dec 15;42(4):560-7. PubMed PMID: 9827680.

[135]Zhang X, Chen X, Yang T, Zhang N, Dong L, Ma S, Liu X, Zhou M, Li B. The effects of different crossing-linking conditions of genipin on type I collagen scaffolds: an in vitro evaluation. *Cell Tissue Bank*. 2014 Dec;15(4):531-41. doi: 10.1007/s10561-014-9423-3. Epub 2014 Jan 18. PubMed PMID: 24442821.

[136]Yuan JM, Chyan CL, Zhou HX, Chung TY, Peng H, Ping G, Yang G. The effects of macromolecular crowding on the mechanical stability of protein molecules. *Protein Sci*. 2008 Dec;17(12):2156-66. doi: 10.1110/ps.037325.108. Epub 2008 Sep 9. PMID: 18780817; PMCID: PMC2590915.

[137]Zhou HX, Rivas G, Minton AP. Macromolecular crowding and confinement: biochemical, biophysical, and potential physiological consequences. *Annu Rev Biophys*. 2008;37:375-97. doi: 10.1146/annurev.biophys.37.032807.125817. Review. PubMed PMID: 18573087; PubMed Central PMCID: PMC2826134.